International Journal of Nanomedicine

Dovepress
open access to scientific and medical research

Open Access Full Text Article

ORIGINAL RESEARCH

Reduced graphene oxide–silver nanoparticle nanocomposite: a potential anticancer nanotherapy

This article was published in the following Dove Press journal:
International Journal of Nanomedicine
5 October 2015
Number of times this article has been viewed

Sangiliyandi Gurunathan
Jae Woong Han
Jung Hyun Park
Eunsu Kim
Yun-Jung Choi
Deug-Nam Kwon
Jin-Hoi Kim

Department of Animal Biotechnology, Konkuk University, Seoul, Republic of Korea

Background: Graphene and graphene-based nanocomposites are used in various research areas including sensing, energy storage, and catalysis. The mechanical, thermal, electrical, and biological properties render graphene-based nanocomposites of metallic nanoparticles useful for several biomedical applications. Epithelial ovarian carcinoma is the fifth most deadly cancer in women; most tumors initially respond to chemotherapy, but eventually acquire chemoresistance. Consequently, the development of novel molecules for cancer therapy is essential. This study was designed to develop a simple, non-toxic, environmentally friendly method for the synthesis of reduced graphene oxide–silver (rGO–Ag) nanoparticle nanocomposites using *Tilia amurensis* plant extracts as reducing and stabilizing agents. The anticancer properties of rGO–Ag were evaluated in ovarian cancer cells.

Methods: The synthesized rGO–Ag nanocomposite was characterized using various analytical techniques. The anticancer properties of the rGO–Ag nanocomposite were evaluated using a series of assays such as cell viability, lactate dehydrogenase leakage, reactive oxygen species generation, cellular levels of malonaldehyde and glutathione, caspase-3 activity, and DNA fragmentation in ovarian cancer cells (A2780).

Results: AgNPs with an average size of 20 nm were uniformly dispersed on graphene sheets. The data obtained from the biochemical assays indicate that the rGO–Ag nanocomposite significantly inhibited cell viability in A2780 ovarian cancer cells and increased lactate dehydrogenase leakage, reactive oxygen species generation, caspase-3 activity, and DNA fragmentation compared with other tested nanomaterials such as graphene oxide, rGO, and AgNPs.

Conclusion: *T. amurensis* plant extract-mediated rGO–Ag nanocomposites could facilitate the large-scale production of graphene-based nanocomposites; rGO–Ag showed a significant inhibiting effect on cell viability compared to graphene oxide, rGO, and silver nanoparticles. The nanocomposites could be effective non-toxic therapeutic agents for the treatment of both cancer and cancer stem cells.

Keywords: graphene–silver nanocomposites, silver nanoparticles, ovarian cancer cells, cancer stem cells, cell viability, caspase-3

Introduction

Graphene is a single, tightly packed monolayer of carbon atoms arranged in a two-dimensional honeycomb network of sp^2 hybridized carbon atoms.[1] Graphene has recently attracted considerable attention in scientific and industrial research areas due to it's excellent properties, such as high electron mobility, excellent mechanical stiffness, extraordinary electronic transport, and high electrical conductivity.[2–4] The graphene material is used in nanoelectronics,[5] nanocomposites,[6] and energy-storage devices.[7,8] Further, graphene has recently been researched in biological applications; in addition to the physical and

Correspondence: Sangiliyandi Gurunathan; Jin-Hoi Kim
Department of Animal Biotechnology, Konkuk University, 1 Hwayang-dong, Gwangjin-gu, Seoul 143-701, Republic of Korea
Tel +82 2 450 3687
Fax +82 2 544 4645
Email gsangiliyandi@yahoo.com; jhkim541@konkuk.ac.kr

chemical properties already mentioned, the nanomaterial has excellent biological properties such as antibacterial,[9–11] biosensing,[12] cellular imaging, and drug delivery capabilities,[13] as well as displaying anticancer activity.[14–17]

A limited number of studies have reported the anticancer activity of graphene or graphene oxide (GO). The anticancer behavior of a novel GO–hypocrellin A hybrid was superior to that of free hypocrellin A in aqueous solution.[18] A GO-TiO_2 hybrid caused significant elevation in caspase-3 activity inducing apoptotic death; the hybrid showed excellent photodynamic anticancer activity without dark cytotoxicity.[19,20] Hu et al[19] and Wang et al[20] demonstrated the dual functionality of graphene quantum dots as targeted anticancer drug carriers and DNA cleavage activity enhancers, which could be useful in cancer therapy. Transferrin-conjugated polyethylene glycolated GO was demonstrated as an efficient nanovector for the targeted delivery of anticancer drugs to brain tumors both in in vitro and in vivo conditions.[21,22] Cheng et al showed a novel pH-sensitive nanostructured antitumor drug from a GO-CONH-Schiff base compound in which chitosan-xanthone Schiff base and GO acted as the tumor inhibitor and drug delivery carrier, respectively.[21]

GO is used as a precursor for reduced GO (rGO) as it is strongly hydrophilic and generates stable and homogeneous colloidal suspensions of negatively charged GO sheets in aqueous and polar organic solvents.[5] The subsequent deoxygenation of GO is necessary by chemically reducing oxygen-containing groups. Maintaining the individual separation of the graphene sheets is the most important and challenging part of the rGO production process.[23] GO reduction by chemical methods results in the formation of limited solubility or even irreversible agglomerates of rGO during preparation in water and most organic solvents (unless capping reagents are used) because of the strong π–π stacking tendency between rGO sheets.[24–26] Agglomeration of rGO can be limited by attaching other molecules or polymers to the sheets. The most commonly used chemical reducing agents are hydrous hydrazine,[27] hydrazine monohydrate, sodium borohydride, and hydrogen sulfide, which are highly toxic to living organisms and the environment.[14,28] Several laboratories have developed biological reducing and stabilizing agents, such as ascorbic acid,[29] amino acids,[30] melatonin,[31] glucose,[14] humanin,[32] microorganisms,[33–35] and plant extracts.[16]

Ag nanoparticles (AgNPs) exhibit very small sizes and large surfaces compared to the bulk metal. For several decades, AgNPs have been of considerable interest in several areas of research, including optics, electronics, magnetics, mechanics, catalysis, energy science, nanobiotechnology, and nanomedicine – particularly as antimicrobial agents for diagnostic purposes.[36] AgNPs also have potential applications in surface enhanced Raman scattering,[37] catalysis,[38] nanoscale electronics,[39] and imaging.[40] Several studies have reported the use of AgNPs as anticancer[41] and antiangiogenic agents in retinal endothelial cells. AgNPs showed significant toxicity in various human cell lines such as human lung fibroblast cells (IMR-90) and human glioblastoma cells (U251),[42] endothelial cells,[43] and MDA-MB-231 human breast cancer cells.[44] However, Ag and graphene as individual agents both show weaker biological activity than graphene–silver nanocomposites. Yu et al[45] showed the enhanced antibacterial activity of AgNPs/halloysite nanotubes/graphene nanocomposites against *Escherichia coli* and *Staphylococcus aureus.* Several previous studies reported the toxicity of GO and graphene-related materials in human cells, including neural pheochromocytoma-derived PC12,[46] human lung epithelial cells or fibroblasts,[47] A549 cells,[48] MCF-7 cells,[17] and MDA-MB-231 human breast cancer cells.[16] No study has yet detailed the use of graphene–AgNP nanocomposites in ovarian cancer cells.

The synthesis of graphene composites with various metal NPs has recently generated extensive interest for the novel optical, electronic, mechanical, and catalytic properties of the composites.[8,49–51] AgNP-decorated graphene is most promising for optoelectronics,[51] catalysis,[52] and electrochemistry[53] applications; it also shows enhanced antibacterial activity.[45,54,55] Therefore, the fabrication of graphene–Ag nanocomposites is of great interest. Until now, most studies focused on the synthesis of AgNPs–graphene composites used hazardous reducing agents such as sodium borohydride, formaldehyde, and hydrazine. These synthesis processes involve multiple steps and complex operations.[8,54,56,57] The use of surfactants as stabilizing agent molecules, which are strongly absorbed on the surface of the metal NPs, decreases the performance of the metal nanoparticle–rGO composite.[58] Efforts have focused on the synthesis of metal nanoparticle–rGO composites by physical and chemical methods. Few studies have exploited green synthesis methods to produce AgNP–rGO films.[59]

No data exist concerning the biological activity of rGO–Ag nanocomposites in human cancer cells and cancer stem cells (CSCs), particularly in human ovarian cancer cells. It is clinically necessary to identify possible new therapeutic molecules that may significantly enhance cancer cell apoptosis. These aspects of nanomedicine remain subjects of particular interest.

Ovarian cancer accounts for approximately 3% of cancers among women; it primarily develops in women over the age of 50. Most ovarian cancer cells are initially chemosensitive,

as evidenced by high initial chemotherapy response rates; however, high recurrence rates suggest the development of chemoresistance. To address the anticancer activity of rGO–Ag nanocomposites, the well-characterized human ovarian cancer cell line A2780 served as a biological model in the in vitro experiments presented here. The A2780 cell lines are poorly differentiated, highly tumorigenic, and heterogeneous with certain phenotypic subsets attributable to CSC-like properties.[60–62]

Considering the current state of nanomedical research, we chose the following objectives. The first goal of this study aimed to develop a simple, non-toxic, cost-effective, quick, and environmentally friendly synthesis approach for rGO–Ag nanocomposites using *Tilia amurensis* plant extracts (TAPE). The second objective was to determine the efficacy of the rGO–Ag nanocomposite in the ovarian cancer cell line A2780 using an in vitro model system.

Materials and methods

Penicillin–streptomycin solution, trypsin–EDTA solution, Dulbecco's Modified Eagle's Medium (DMEM), Roswell Park Memorial Institute (RPMI) 1640 medium, and 1% antibiotic–antimycotic solution were obtained from Thermo Fisher Scientific (Waltham, MA, USA). Polyethylene, $AgNO_3$, fetal bovine serum, and the in vitro toxicology assay kit were purchased from Sigma-Aldrich Co. (St Louis, MO, USA). Graphite (Gt) powder, NaOH, $KMnO_4$, $NaNO_3$, anhydrous ethanol, 98% H_2SO_4, 36% HCl, 30% H_2O_2 aqueous solution, and all other chemicals were purchased from Sigma-Aldrich Co., unless otherwise stated.

Synthesis of AgNPs

The synthesis of AgNPs was conducted according to the method described previously.[63] *T. amurensis* leaves were collected at the Konkuk University campus in Seoul, Republic of Korea, and stored at 4°C until needed. Twenty grams of *T. amurensis* leaves were washed thoroughly with double-distilled water, and then sliced into fine pieces, approximately 1–5 cm, using a sharp stainless steel knife. The finely cut *T. amurensis* leaves were suspended in 100 mL sterile distilled water and boiled for 5 minutes. The resulting mixture was filtered through a Whatman number 1 filter paper. The filtered extract was used for the synthesis of AgNPs by adding 10 mL to 100 mL 5 mM aqueous $AgNO_3$; the mixture was incubated for 6 hours at 60°C at pH 8.0. The bio-reduction of the silver ions was monitored spectrophotometrically at 420 nm. Further characterizations of the synthesized AgNPs were performed as described previously.[64]

Synthesis of GO

GO was synthesized as described previously[10,65,66] with suitable modifications. In a typical synthesis process, 2 g natural Gt powder was added to 350 mL H_2SO_4 at 0°C; 8 g $KMnO_4$ and 1 g $NaNO_3$ were added gradually while stirring. The mixture was transferred to a 40°C water bath and stirred for 60 minutes. Deionized water (250 mL) was slowly added and the temperature was increased to 98°C. The mixture was maintained at 98°C for 30 minutes; the reaction was terminated by the addition of 500 mL deionized water and 40 mL 30% H_2O_2 solution. The color of the mixture changed to brilliant yellow, indicating the oxidation of pristine Gt to Gt oxide. The mixture was filtered and washed with diluted HCl to remove metal ions. The product was washed repeatedly with distilled water until a pH of 7.0 was achieved; the synthesized Gt oxide was further sonicated for 15 minutes.

Reduction of GO by TAPE

The reduction of GO was accomplished as described earlier.[16] Briefly, rGO was obtained from the reaction of TAPE with GO. In a typical reduction experiment, 10 mL TAPE was added to 90 mL 1.0 mg/mL aqueous GO; the mixture was sealed tightly in a glass bottle and stirred at 30°C for 12 hours. Subsequently, by using a magneto-stirrer heater, the rGO suspension was stirred at 400 rpm at a temperature of 30°C for 30 minutes. A homogeneous TAPE–rGO suspension was obtained without aggregation. The obtained material was washed with distilled water several times to remove the excess TAPE residue and re-dispersed in water by sonication. The suspension was centrifuged at 5,000 rpm for 30 minutes; the final product was collected by vacuum filtration and vacuum-dried.

Synthesis of rGO–Ag nanocomposite

Synthesized rGO–Ag nanocomposites were prepared using TAPE. An aqueous solution of 100 mg GO and 5 mM of $AgNO_3$ was used as precursors for the rGO–Ag nanocomposites. Initially, 100 mg GO was dispersed in 60 mL water by 60 minutes sonication. The reaction mixture was prepared in a 250 mL round bottom flask by dissolving 5 mM $AgNO_3$ in 30 mL water. To this solution, 60 mL GO dispersion and 10 mL of aqueous TAPE were added and the mixture was stirred at 90°C for 12 hours. After 12 hours, the reaction was stopped and the resultant mixture was washed three times with water using centrifugation. The product was obtained as a black powder and used for further experiments.

Characterization of rGO and rGO–Ag nanocomposite

GO, rGO, and the rGO–Ag nanocomposite were characterized according to the methods described previously.[16,67] Ultraviolet-visible (UV-Vis) spectra of GO, rGO, and rGO–Ag were recorded using an OPTIZEN POP spectrophotometer (Mecasys Co., Seoul, Republic of Korea). X-ray diffraction (XRD) analyses were performed in a Bruker D8 DISCOVER X-ray diffractometer (Bruker AXS GmBH, Karlsruhe, Germany). The X-ray source was 3 kW with a Cu target; high-resolution XRD patterns were measured using a scintillation counter (λ=1.5406 Å). The XRD was run at 40 kV and 40 mA, and samples were recorded at 2θ values between 10° and 80°. The dried powders of GO, rGO, and rGO–Ag nanocomposite were diluted with KBr to perform Fourier transform infrared (FTIR) spectroscopy (PerkinElmer Inc., Waltham, MA, USA) and spectrum GX spectrometry within a range of 500–4,000 cm^{-1}. A JSM-6700F semi-in-lens field emission scanning electron microscope (SEM) (JEOL, Tokyo, Japan) was used to acquire SEM images. The solid samples were transferred to a carbon tape held in an SEM sample holder, and the analyses were performed at an average working distance of 6 mm. Transmission electron microscopy (TEM; Hitachi H-7500, Hitachi Ltd., Tokyo, Japan) was used to determine the size and morphology of the dispersed AgNPs. Raman spectra of GO, rGO, and rGO–Ag were measured using a WITEC Alpha300 laser with a wavelength of 532 nm. The calibration was initially performed using an internal Si reference at 500 cm^{-1}, yielding a peak position resolution of less than 1 cm^{-1}. The spectra were measured from 500 to 4,500 cm^{-1}. All samples were deposited on glass slides in powdered form without a solvent.

Cell culture and exposure of ovarian cancer cells A2780 to rGO–Ag nanocomposite

Human ovarian cancer cells A2780 were cultured in DMEM supplemented with 10% fetal bovine serum, 2 mM glutamine, and 100 U/mL penicillin–streptomycin in a humidified 5% CO_2 incubator at 37°C. At approximately 75% confluence, the cells were harvested using 0.25% trypsin and subcultured in 75 cm^2 flasks, six-well plates, or 96-well plates, depending on the intended use. The cells were allowed to attach to the substratum for 24 hours prior to treatment. The medium was replaced three times per week, and the cells were passaged at subconfluency. The cells were prepared in 100 µL aliquots at a density of 1×10^5 mL^{-1} and plated in 96-well plates. After the cells were cultured for 24 hours, the medium was replaced with a medium containing GO (0–100 µg/mL), rGO (0–50 µg/mL), rGO–Ag (0–25 µg/mL), or AgNPs (0–50 µg/mL). After incubation for an additional 24 hours, the cells were analyzed for viability. The cells that were not exposed to GO, rGO, rGO–Ag, or AgNPs served as controls.

Cell viability assay

The WST-8 assay was performed as described previously.[16,44] Typically, 1×10^4 cells were seeded in a 96-well plate and cultured in DMEM supplemented with 10% fetal bovine serum at 37°C under 5% CO_2. After 24 hours, the cells were washed twice with 100 µL of serum-free DMEM and incubated with 100 µL of different concentrations of GO, rGO, rGO–Ag, or AgNPs, as described above. After 24 hours of exposure, the cells were washed twice with serum-free DMEM, and 15 µL of WST-8 solution was added to each well containing 100 µL of serum-free DMEM. After 1 hour of incubation at 37°C under 5% CO_2, 80 µL of the mixture was transferred to another 96-well plate. The absorbance of the mixture solutions was measured at 450 nm using a microplate reader. Cell-free control experiments were performed to determine the reactivity of the GO, rGO, rGO–Ag, and AgNPs with the WST-8 reagents. Typically, 100 µL of GO, rGO, rGO–Ag, or AgNP suspensions with different concentrations was added to a 96-well plate and 10 µL of WST-8 reagent solution was added to each well; the mixture was incubated at 37°C under 5% CO_2 for 1 hour. After incubation, the GO, rGO, rGO–Ag, or AgNPs were centrifuged, and 100 µL of the supernatant was transferred to another 96-well plate. The optical density was measured at 450 nm.

Cell morphology

Ovarian cancer cells were plated in six-well plates (1×10^4 cells per well) and incubated with the respective inhibitory concentration $(IC)_{50}$ concentrations of GO, rGO, rGO–Ag, or AgNPs for 24 hours. Cells cultured in a medium without the addition of GO, rGO, rGO–Ag, or AgNPs were used as the control. Cell morphology was analyzed using an optical OLYMPUS IX71 microscope (Olympus Corporation, Tokyo, Japan) at 24 hours post-treatment using the appropriate filter sets.

Membrane integrity

The cell membrane integrity of the human ovarian cancer cells was evaluated by determining the activity of lactate dehydrogenase (LDH) leaking out of the cells according to the manufacturer's instructions (in vitro toxicology assay kit, TOX7; Sigma-Aldrich Co.) and also as described previously.[16,44] Briefly, the cells were exposed to the

respective IC_{50} concentrations of GO, rGO, rGO–Ag, or AgNPs for 24 hours, and then 100 µL per well of each cell-free supernatant was transferred in triplicate into the wells of a 96-well plate; subsequently, 100 µL of the LDH assay reaction mixture was added to each well. After 3 hours of incubation under standard conditions, the optical density of the color generated was determined at a wavelength of 490 nm using a microplate reader.

Determination of ROS

Reactive oxygen species (ROS) was estimated according to a method described previously.[16,44] Intracellular ROS was measured based on the intracellular peroxide-dependent oxidation of 2′,7′-dichlorodihydrofluorescein diacetate (DCFH-DA, Molecular Probes, Thermo Fisher Scientific, Waltham, MA, USA) to form the fluorescent compound 2′,7′-dichlorofluorescein, as previously described. The cells were seeded onto 24-well plates at a density of 5×10^4 cells per well and cultured for 24 hours. After washing twice with phosphate-buffered saline (PBS), fresh media containing respective IC_{50} concentrations of GO, rGO, rGO–Ag, or AgNPs were added and incubated for 24 hours. The cells were then supplemented with 20 µM DCFH-DA, and the incubation continued for 30 minutes at 37°C. The cells were rinsed with PBS, 2 mL of PBS was added to each well, and the fluorescence intensity was determined using a spectrofluorometer (Gemini EM) with excitation at 485 nm and emission at 530 nm.

Determination of MDA

Malonaldehyde (MDA) was measured according to the method described earlier[68] with slight modifications. The A2780 cells were seeded into six-well microplates at 2.0×10^6 cells per well. The cells were treated with the respective IC_{50} concentrations of GO, rGO, rGO–Ag, or AgNPs for 24 hours. After incubation, the cells were harvested and washed twice with an ice-cold PBS solution. The cells were collected and disrupted by ultrasonication for 5 minutes on ice. The cell extract (100 µL) was used to detect MDA according to the procedure recommended by the manufacturer of the MDA assay kit (Sigma, St Louis, USA). The concentration of MDA was measured on a microplate reader at a wavelength of 530 nm. The protein concentration was determined using the Bio-Rad protein assay kit (Bio-Rad Laboratories Inc., Hercules, CA, USA).

Determination of GSH

The cellular extract was prepared similar to that used to measure MDA. The concentration of glutathione (GSH) was expressed as nmol per milligram of protein. The cell suspension (100 µL) was mixed with 100 µL of precipitant and centrifuged at 5,000 rpm for 10 minutes. After centrifugation, 100 µL supernatant was used for the GSH assay, performed according to the manufacturer's protocol. The reaction was monitored at 405 nm in a microplate reader. The protein concentration was determined using the Bio-Rad protein assay kit (Bio-Rad Laboratories Inc.).

Measurement of caspase-3 activity

The measurement of caspase-3 was performed according to the method described earlier.[45] The cells were treated with the respective IC_{50} concentrations of GO, rGO, rGO–Ag, and AgNPs or caspase-3 inhibitor for 24 hours. The activity of caspase-3 was measured in the cancer cells using a kit from Sigma-Aldrich Co., according to the manufacturer's instructions. The cells were washed with ice-cold PBS and lysed with 100 µL of lysis buffer (50 mM Tris-HCl, pH 7.5; 150 mM NaCl; 1 mM ethylene glycol tetraacetic acid; 1 mM NaF; 1% Nonidet P-40; 1 mM phenylmethylsulfonyl fluoride protease inhibitor cocktail) for 30 minutes at 4°C. The protein extracts were collected after centrifugation at 10,000 rpm for 10 minutes. The protein concentration was determined using the Bio-Rad protein assay kit (Bio-Rad Laboratories Inc.). Equal amounts (50 µg) of protein extracts were mixed with the assay buffer (20 mM HEPES, pH 7.4; 100 mM NaCl; 0.1% CHAPS; 10 mM DTT; 1 mM EDTA; 10% sucrose), added to 96-well microtiter plates, and incubated with the caspase-3 substrate (acetyl-Asp-Glu-Val-Asp p-nitroanilide, Ac-DEVD-pNA) and caspase-3 inhibitor (Ac-DEVD-CHO) for 1 hour before the absorbance at 405 nm was read. The calorimetric assay was based on the hydrolysis of the caspase-3 substrate by caspase-3 resulting in the release of the p-nitroaniline (pNA) moiety. The concentration of pNA released from the substrate was calculated from the absorbance values at 405 nm. The assay was done with non-induced cells and also in the presence of the caspase-3 inhibitor (Ac-DEVD-CHO) for a comparative analysis.

TUNEL assay

Apoptosis induced by GO, rGO, rGO–Ag, and AgNPs was determined using the TUNEL assay. Apoptotic cells were determined using a DNA Fragmentation Imaging Kit (Hoffman-La Roche Ltd., Basel, Switzerland) following the manufacturer's instruction. Briefly, 1.5×10^6 A2780 cells per well were cultured in six-well plates to study the apoptosis in adherent cells. Cells were treated with the respective IC_{50} concentrations of GO, rGO, rGO–Ag, and AgNPs for

24 hours. After the incubation period, the culture medium was aspirated and the cell layers trypsinized. The trypsinized cells were reattached on 0.01% polylysine-coated slides, fixed with 4% methanol-free formaldehyde solution, and stained according to the manufacturer's instructions for the TUNEL protocol (Sigma, St Louis, USA). The stained cells were observed with a Carl Zeiss epifluorescence microscope (Axiovert, Carl Zeiss Meditec AG, Jena, Germany) using a triple bandpass filter. To determine the percentage of cells experiencing apoptosis, 1,000 cells were counted in each experiment. Based on the TUNEL reaction using terminal deoxynucleotidyl transferase and fluorescein-labeled dUTP, fluorescence detection of cells with apoptotic DNA strand breaks was performed. To examine the total cell numbers, the nuclei were labeled simultaneously with DAPI (4′,6-diamidino-2-phenylindole). Merged images of both channels were shown using a fluorescence microscope (Olympus Corporation) at 500× magnification.

Statistical analyses

All assays were conducted in triplicate and each experiment was repeated at least three times. The results are presented as means ± standard deviation. All the experimental data were compared using the Student's *t*-test. A *P*-value less than 0.05 was considered statistically significant.

Results and discussion

Synthesis and characterization of rGO–Ag nanocomposite using UV-Vis spectroscopy

The nanocomposite was synthesized by mixing GO and $AgNO_3$ using TAPE as a reducing and stabilizing agent. Figure 1 shows the UV-Vis spectrum of GO, rGO, and the rGO–Ag nanocomposite. GO exhibits two characteristic peaks at 230 and 300 nm, corresponding to the π–π* transitions of aromatic C–C bonds and n–π* transitions of C=O bonds, respectively. The UV-Vis spectrum of rGO exhibits a characteristic band at 261 nm, indicating the restoration of the extensive conjugated sp^2 carbon network.[10,57,69–71] A new peak at 410 nm is observed after the deposition of AgNPs on the rGO surface; the band at 410 nm in the absorption spectrum of the rGO–Ag nanocomposite is attributed to surface plasmons and indicates the presence of AgNPs.[64,69,71,72] The disappearance of the characteristic peaks of rGO and the emergence of a new band originating from AgNPs clearly indicate the simultaneous reduction of both rGO and $AgNO_3$ and the formation of the rGO–Ag composite. Pasricha et al[54] reported the synthesis of Ag–GO nanocomposites under alkaline conditions. $NaBH_4$ was used to reduce Ag ions to generate

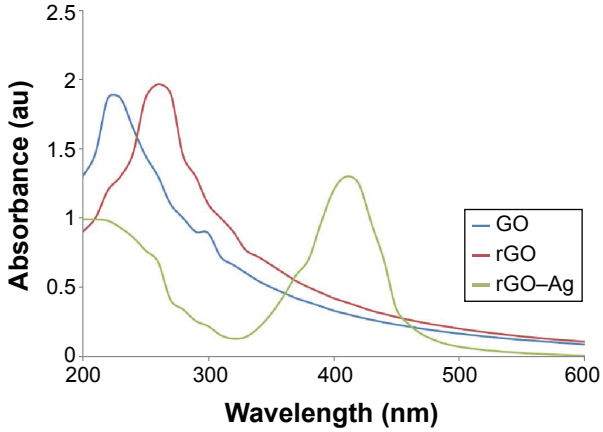

Figure 1 Synthesis and characterization of graphene oxide (GO), reduced graphene oxide (rGO), and rGO–Ag nanocomposite using ultraviolet-visible spectroscopy.
Notes: Spectra of GO exhibit a maximum absorption peak at ~231 nm corresponding to the π–π transitions of aromatic C–C bonds. The absorption peak for rGO is red-shifted to 261 nm. A new peak at 410 nm is observed after deposition of Ag nanoparticles (AgNPs) on the rGO surface; the band at 410 nm in the absorption spectrum of the rGO–Ag nanocomposite is attributed to surface plasmons and the presence of AgNPs. At least three independent experiments were performed for each sample and reproducible results were obtained. The data present the results of a representative experiment.

GO nanosheet-based nanocomposites.[73] Al-Marri et al[74] reported the simultaneous reduction of both GO and Ag ions using *Pulicaria glutinosa* plant extract as the reducing agent. GO–Ag nanocomposites have been prepared with $AgNO_3$ using various reducing agents such as sodium citrate,[69] ammonia,[52] and poly(*N*-vinyl-2-pyrrolidone).[75] However, rGO–Ag nanocomposites can also be obtained using TAPE, which possesses better reducing abilities at normal pH values without requiring alkali and additional reductants as TAPE contains a large amount of natural antioxidants such as alkaloids, tannin, steroids, phenol, saponins, and flavonoids in aqueous extracts. These molecules are demonstrated by the results in Figure 1 to be strong reducing and stabilizing agents, with numerous OH groups found in the extracts. This method provides a simple, easy, and biomolecule-mediated synthesis of rGO–Ag nanocomposites.

XRD analysis of GO, rGO, and rGO–Ag nanocomposite

To support the data obtained by UV-Vis spectroscopy, GO, rGO, and rGO–Ag were further characterized using XRD. The XRD patterns of GO, rGO, and rGO–Ag are shown in Figure 2, which confirms the crystalline nature of the rGO–Ag nanocomposites. GO exhibits a reflection at a low angle (2θ=10.9°) compared with the pattern of pristine Gt (2θ=26.5°). The reflection at 2θ=10.9° in GO disappears and a new reflection emerges at 2θ=26.4°, indicating the reduction of GO. However, in the rGO–Ag nanocomposites,

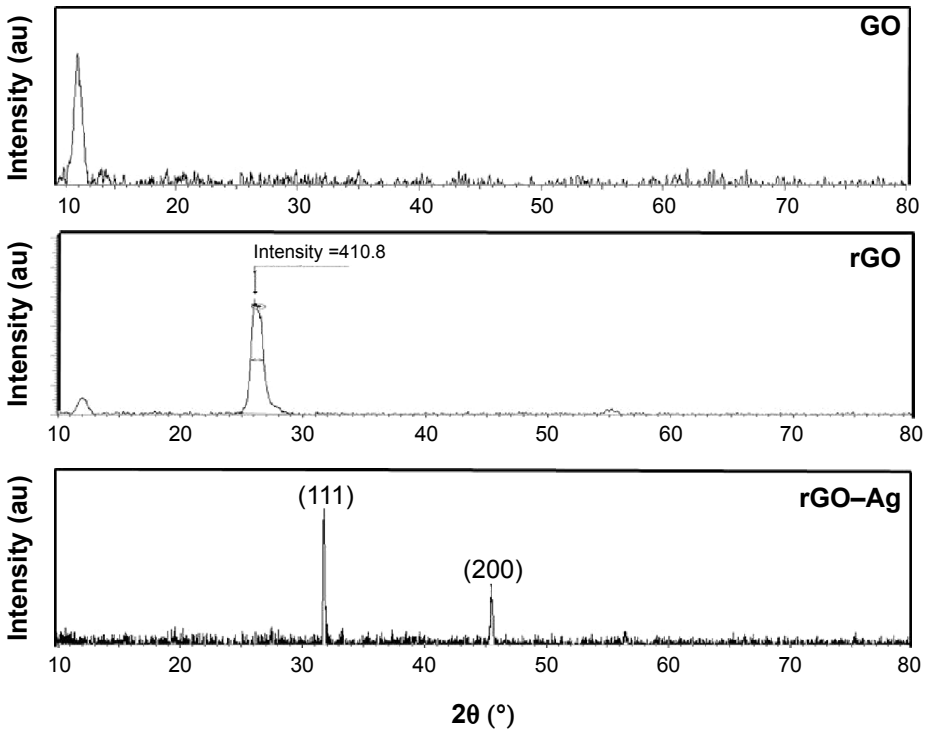

Figure 2 X-ray diffraction (XRD) patterns of graphene oxide (GO), reduced graphene oxide (rGO), and rGO–Ag nanocomposite.
Notes: In the XRD pattern of GO, a strong sharp peak at 2θ=10.9° corresponds to an interlayer distance of 7.6 Å. rGO has a broad peak centered at 2θ=26.4° corresponding to an interlayer distance of 3.6 Å. Apart from the characteristic reflections of rGO (2θ=26.4°), the rGO–Ag nanocomposite shows two different distinct reflections in the diffractogram at 33.1° and 45.3° corresponding to the (111) and (200) planes, respectively, of face centered cubic Ag. At least three independent experiments were performed for each sample and reproducible results were obtained. The data present the results of a representative experiment.

apart from the characteristic reflections of rGO (2θ=26.4°), two different distinct reflections in the diffractogram appear at 33.1° and 45.3°, corresponding to the (111) and (200) planes, respectively, of the cubic Ag crystal of AgNPs (JCPD No 04-0783).[55,69,70,75,76] This confirms the formation of metallic AgNPs after reduction. Compared with the patterns of GO and rGO, the XRD pattern of the rGO–Ag nanocomposite shows clear peaks corresponding to the (111) and (200) diffraction peaks of fcc Ag, confirming that Ag exists in a crystalline state.[55] The absence of any additional reflections besides those of graphene and Ag clearly indicates the reduction of GO and Ag ions and suggests that the rGO–Ag nanocomposite lattice is unaffected by other molecules in the plant extract.[74]

In contrast, GO shows a peak at 10.7° from the stacking of the GO layers, which may be intensified by inter-lamellar water trapped between the hydrophilic GO sheets;[49] the peak disappears after the decoration of GO with AgNPs. The XRD results suggest that Ag ions were reduced and AgNPs formed and then loaded on the surface of the GO sheets, preventing the stacking of the GO layers. This phenomenon may be associated with the destruction of the pre-existing lamellar structure of the GO sample after the incorporation of Ag.[69,70,72]

FTIR analysis of rGO–AgNP nanocomposite

FTIR spectroscopy was used to verify the biomolecule-mediated rGO–Ag nanocomposite synthesis. The FTIR spectra of GO, rGO, and rGO–Ag nanocomposite are shown in Figure 3. The GO spectrum shows dominant peaks at 1,020, 1,200, 1,350, 1,600, 1,720, and 3,430 cm^{-1}. The peak at 1,020 cm^{-1} corresponds to a stretching vibration from the C–O–C bonds of epoxy or alkoxy groups. The peak at 1,200 cm^{-1} is attributed to C–OH bonds, while the peak centered at 1,600 cm^{-1} is assigned to C=C bonds associated with the skeletal vibrations of unoxidized Gt domains. The peak at 1,720 cm^{-1} is attributed to C=O bonds in carboxylic acid and carbonyl moieties.[34,77,78] The adsorption band at approximately 1,600 cm^{-1} corresponds to the C=C bonding of aromatic rings within the GO carbon skeleton structure.[16] Other oxygenated functional groups identified include OH at approximately 3,430 and 1,350 cm^{-1}; C=O at approximately 1,720 cm^{-1}; C–OH at approximately 1,200 cm^{-1}; and C–O at approximately 1,050 cm^{-1}. Notably, the rGO–Ag nanocomposite shows a new band at 1,420 cm^{-1}, resulting from the C–N stretching vibration of TAPE-reduced rGO–Ag. In addition, the rGO–Ag nanocomposite spectrum shows a significant decrease in the intensity of the adsorption

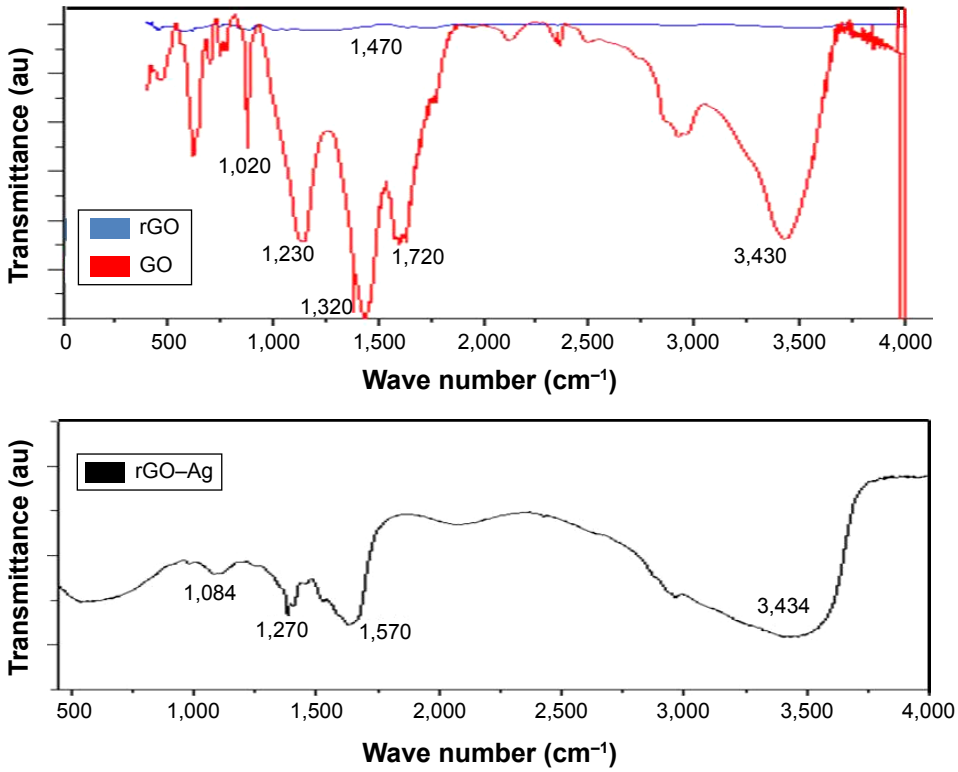

Figure 3 Fourier transform infrared (FTIR) spectra of graphene oxide (GO), reduced graphene oxide (rGO), and rGO–Ag nanocomposite.
Notes: Dried powders of GO, rGO, and rGO–silver nanoparticle (AgNP) nanocomposite were diluted with KBr to perform FTIR spectroscopy and spectrum GX spectrometry within the range of 500–4,000 cm^{-1}.

bands of the oxygenated functional groups; this could result from the interaction of GO with TAPE that produces C=O groups on the surface, the presence of Ag on the rGO surface, or the slight reduction of GO during the synthesis of the rGO–Ag nanocomposite.[79] Similarly, Chook et al[52] reported the synthesis of Ag–GO nanocomposites using glucose as a reducing agent in the presence of an $AgNH_3$ complex with a GO suspension. In the FTIR spectrum of the rGO–Ag nanocomposite, the peaks at 1,020, 1,230, 1,320, 1,720, and 3,430 cm^{-1} are relatively weak compared to those of GO. Furthermore, the absorption peak at approximately 1,270 cm^{-1} is attributed to the C–OH bond, and the new absorption band at 1,570 cm^{-1} is attributed to the skeletal vibration of the graphene sheets.[71,80] These results clearly demonstrate that GO was successfully exfoliated and reduced to graphene and that strong interactions may exist between AgNPs and the remaining surface hydroxyl groups.[81]

SEM analysis of GO, rGO, and rGO–Ag nanocomposite

Figure 4 shows the SEM images of GO (Figure 4a), rGO (Figure 4b), and rGO-Ag (Figure 4c). GO shows a closely packed lamellar structure and a flaky texture, reflecting the multilayered microstructure (Figure 4A). The GO samples contain several layers of aggregated and square-shaped crumpled sheets closely associated with each other to form a continuous conducting network.[10,65,67] With the exfoliation of Gt into GO, the edges of the GO sheets become crumpled, folded, and closely restacked, and the surface of GO exhibits a soft carpet-like morphology, possibly because of the presence of residual H_2O molecules and hydroxyl or carboxyl groups.[82] In contrast to GO, rGO exhibits transparent rippled silk-like waves or a flaky, scale-like, layered structure.[16] These observations agree well with a previous study in which graphene sheets obtained from GO by rapid thermal expansion in atmospheric N_2 showed curled morphologies consisting of thin, wrinkled, paper-like structures, with fewer layers (approximately four) and larger specific surface areas than GO.[83] Figure 4C shows typical SEM images of the as-prepared rGO–Ag hybrids; well-dispersed AgNPs with sizes from 10 to 20 nm are deposited on the graphene. Interestingly, in the rGO doped with Ag particles and reduced, the Ag crystallites are deposited on graphene surfaces as spacers between neighboring sheets, and a curled and wavy morphology is observed. The AgNPs are well separated from each other and randomly distributed

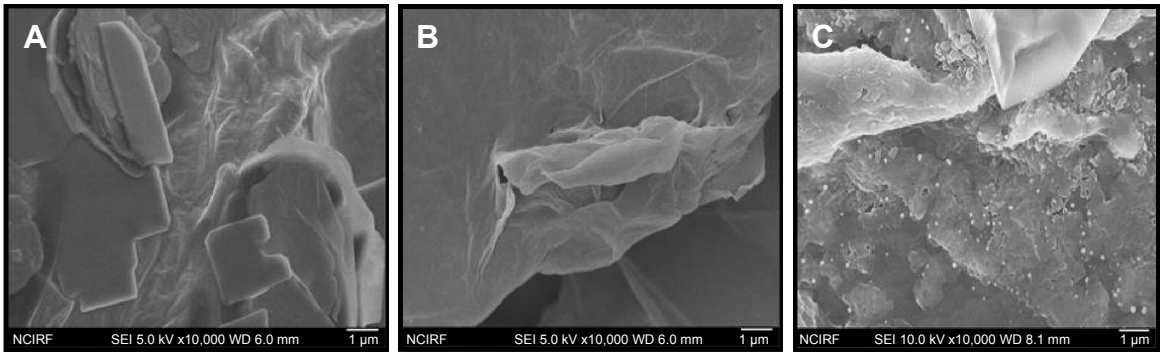

Figure 4 SEM images of GO, rGO, and rGO–Ag nanocomposite.
Notes: Representative SEM images of (**A**) GO, (**B**) rGO, and (**C**) rGO–Ag nanocomposite dispersions at 500 µg/mL.
Abbreviations: SEM, scanning electron microscopy; GO, graphene oxide; rGO, reduced graphene oxide.

on the graphene sheets as spacers keeping the neighboring sheets separate.

Analysis of surface morphological features of GO, rGO, and rGO–Ag by TEM

The morphological features of GO, rGO, and the rGO–Ag nanocomposite were determined by TEM analysis. Figure 5 shows typical TEM images of GO, rGO, and rGO–Ag; GO exhibits a closely packed lamellar and plate structure with a clean surface. In contrast to GO, rGO shows a typical sheet-like structure with a size of 100 nm. The synthesis of smaller GO sheets is extremely tedious; these results show that the synthesis method may be useful for several applications. In addition, the rGO–Ag nanocomposite shows many NPs anchored to the surfaces of both samples. The adhered NPs have spherical morphologies, an even distribution, and a homogeneous dispersion on the rGO surfaces; most of the NPs have a diameter of 20 nm. In addition, the presence of evenly distributed silky waves of rGO sheets can be observed. As shown in Figure 5, well-dispersed AgNPs are homogeneously deposited on rGO sheets with sizes uniformly distributed around 20 nm. On the surface of the rGO–Ag nanocomposite, the sheets exhibit very clean silky and wavy structures. These may be important for preventing the aggregation of rGO and maintaining a surface facilitating the attachment of AgNPs to the graphene sheets. The TEM image of the rGO–Ag nanocomposite clearly indicates strong interactions between the AgNPs and GO because almost all AgNPs are distributed within the GO sheets and very few AgNPs reside outside the GO support.[75]

Recently, Yuan et al[81] fabricated graphene/Ag nanocomposites (GNS/AgNPs) via a green and facile method employing GO as a precursor of graphene, $AgNO_3$ as a precursor of AgNPs, and sodium citrate as the reducing and stabilizing agent. Chook et al[52] demonstrated the fabrication of AgNPs and Ag–GO nanocomposites by green microwave irradiation; the resulting Ag–GO samples showed the deposition of AgNPs with an average size of 40.7±7.5 nm on the GO sheets. The presence of transparent and uniform silk waves of rGO sheets can also be observed and attributed to

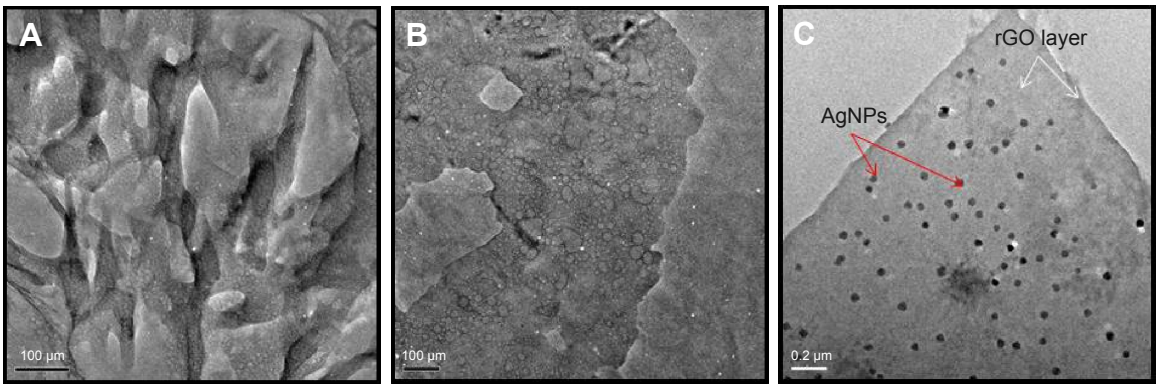

Figure 5 TEM images of (**A**) GO, (**B**) rGO, and (**C**) rGO–Ag nanocomposite.
Abbreviations: TEM, transmission electron microscopy; GO, graphene oxide; rGO, reduced graphene oxide; AgNPs, silver nanoparticles.

the deposition of AgNPs on the surface of the GO sheets. Yun et al[84] reported thiolated carbon nanotube (CNT)–Ag and GO–Ag surfaces with average sizes of 2 to 4 nm. Hu et al[75] fabricated rGO and AgNPs using poly(*N*-vinyl-2-pyrrolidone) as a reductant and stabilizer. The prepared rGO–Ag nanocomposite showed nearly transparent GO sheets decorated with large amounts of well-dispersed AgNPs with average sizes of 13 nm and confined within the rGO sheets.

de Faria et al[69] reported the preparation and mechanisms of GO decorated with biogenic AgNPs with an average size of 3.5 nm. During the chemical synthesis of the GO–Ag nanocomposites, the AgNPs were attached to GO via the interaction of the Ag ions with the oxygenated groups on the GO surface; the carboxylic, epoxy, and hydroxyl groups could have provided sites for the anchoring and growth of the AgNPs.[54,76,85] de Faria et al[69] proposed a possible mechanism of GO–Ag synthesis using biological molecules in which a protein surrounding the metallic NPs could interact with oxygenated groups to allow the anchoring of AgNPs on the GO surface. The data from our experiments suggest similar mechanisms for rGO–Ag nanocomposite synthesis in which the amine groups available in TAPE could be involved in the interaction of Ag with the oxygenated groups of GO.

Raman spectroscopy analysis of GO, rGO, and rGO–Ag nanocomposite

Raman spectroscopy was used to analyze information related to the electronic and structural properties of GO, rGO, and rGO–Ag nanocomposite as it is a powerful nondestructive tool for the characterization of carbonaceous materials and distinguishing ordered and disordered carbon structures.[71,86,87] This technique provided additional evidence of the reducing ability of TAPE for GO and $AgNO_3$. As shown in Figure 6, in the Raman spectrum of GO, the G band is broadened and shifted to 1,599 cm^{-1} while a broadened D band at 1,347 cm^{-1} also appears (Figure 6A). After the GO reduction, the Raman spectrum of rGO shows a G band at 1,584 cm^{-1} and a D band at 1,351 cm^{-1} (Figure 6B). The Raman spectrum shows that the typical features of rGO are a D band at approximately 1,351 cm^{-1} and a G band at approximately 1,584 cm^{-1}. The D band is assigned to the breathing mode of the k-point phonons with A_{1g} symmetry, whereas the G band introduces the E_{2g} phonon of the carbon sp^2 atoms.[88,89] The prominent D peak is derived from the structural imperfections created by the attachment of hydroxyl and epoxide groups on the carbon basal plane. In the corresponding Raman spectra, the G bands of rGO and rGO–Ag are broadened because of the enhanced isolated double bonds, whereas the D bands intensify because of the enhanced disorder of the rGO and rGO–Ag nanocomposite. As shown in Figure 6C, the G band of the rGO–Ag nanocomposite at 1,611 cm^{-1} is clearly upshifted by 27 cm^{-1} with respect to that of rGO (1,584 cm^{-1}), consistent with previous research showing that the introduction of Au caused the upshift of the G band by electron–phonon coupling.[55] Wang et al[90] also showed that the G band of the Au–rGO nanocomposite was clearly upshifted by 11 cm^{-1} with respect to that of GO. The intensity ratio of the D to G bands (I_D/I_G) is often used as a measure of the defect

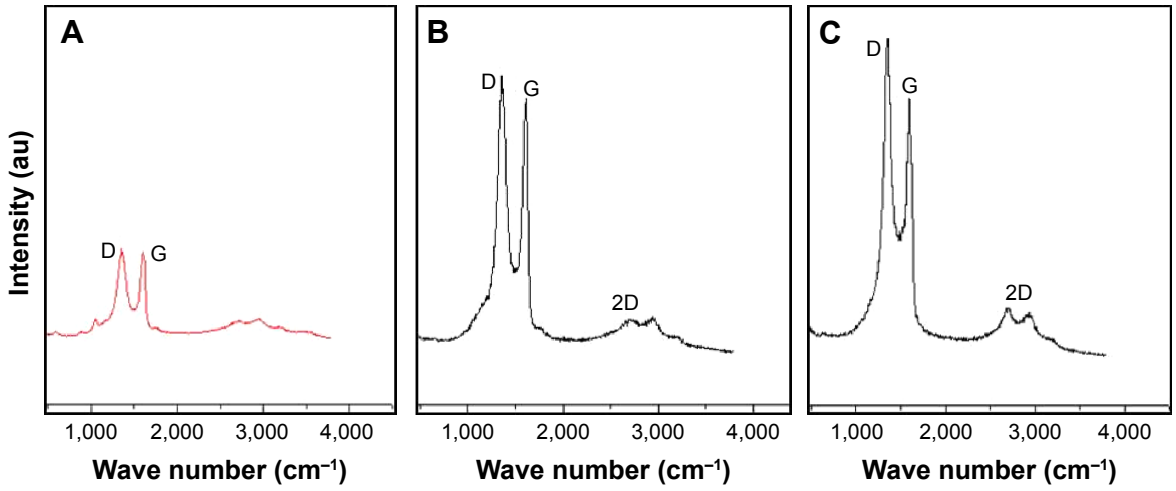

Figure 6 Raman spectroscopy analyses of (**A**) graphene oxide (GO), (**B**) reduced graphene oxide (rGO), and (**C**) rGO–Ag nanocomposite.
Notes: Raman spectra of (**A**) GO, (**B**) rGO, and (**C**) rGO–Ag nanocomposite were obtained using a laser excitation wavelength of 532 nm at the power of 1 mW after the removal of background fluorescence. The intensity ratio of the D to G bands (I_D/I_G) increases to 2.09 (rGO–Ag nanocomposite) from 1.74 (rGO) and 1.54 (GO). At least three independent experiments were performed for each sample and reproducible results were obtained.

levels in graphitic systems.[90] Upon the introduction of Ag, the ratio of I_D/I_G increases to 2.09 (rGO–Ag nanocomposite) from 1.74 (rGO) and 1.54 (GO), indicating that the size of the sp^2 domain decreases as the graphene sheet is broken into fragments during the AgNP treatment. In addition, the presence of rGO–Ag in the composites enhances the relative intensity ratio of D/G, which represents the degree of disorder. The 2D band is well known for distinguishing the thickness of the graphene sheets. For the simultaneous reductions of GO and AgNPs by TAPE, a broad 2D band at 2,672 cm^{-1} for the rGO–Ag nanocomposites is observed, confirming the presence of a few layers of graphene sheets in the as-prepared nanocomposite.

Dose-dependent effect of rGO–Ag nanocomposite on cell viability of ovarian cancer cells

The as-prepared rGO–Ag nanocomposite materials showed significant stability and solubility in water with no aggregation after 3 months owing to the strong interactions between the rGO sheets and Ag molecules.[79] To show the potential applications of the rGO–Ag nanocomposite as an anticancer agent, the in vitro cytotoxicity of the rGO–Ag nanocomposite on ovarian cancer cells was determined using the MTT assay. Here, we evaluated the efficiency of the rGO–Ag nanocomposite as a potential inhibitory agent for ovarian cancer cells and used three different nanomaterials of GO,

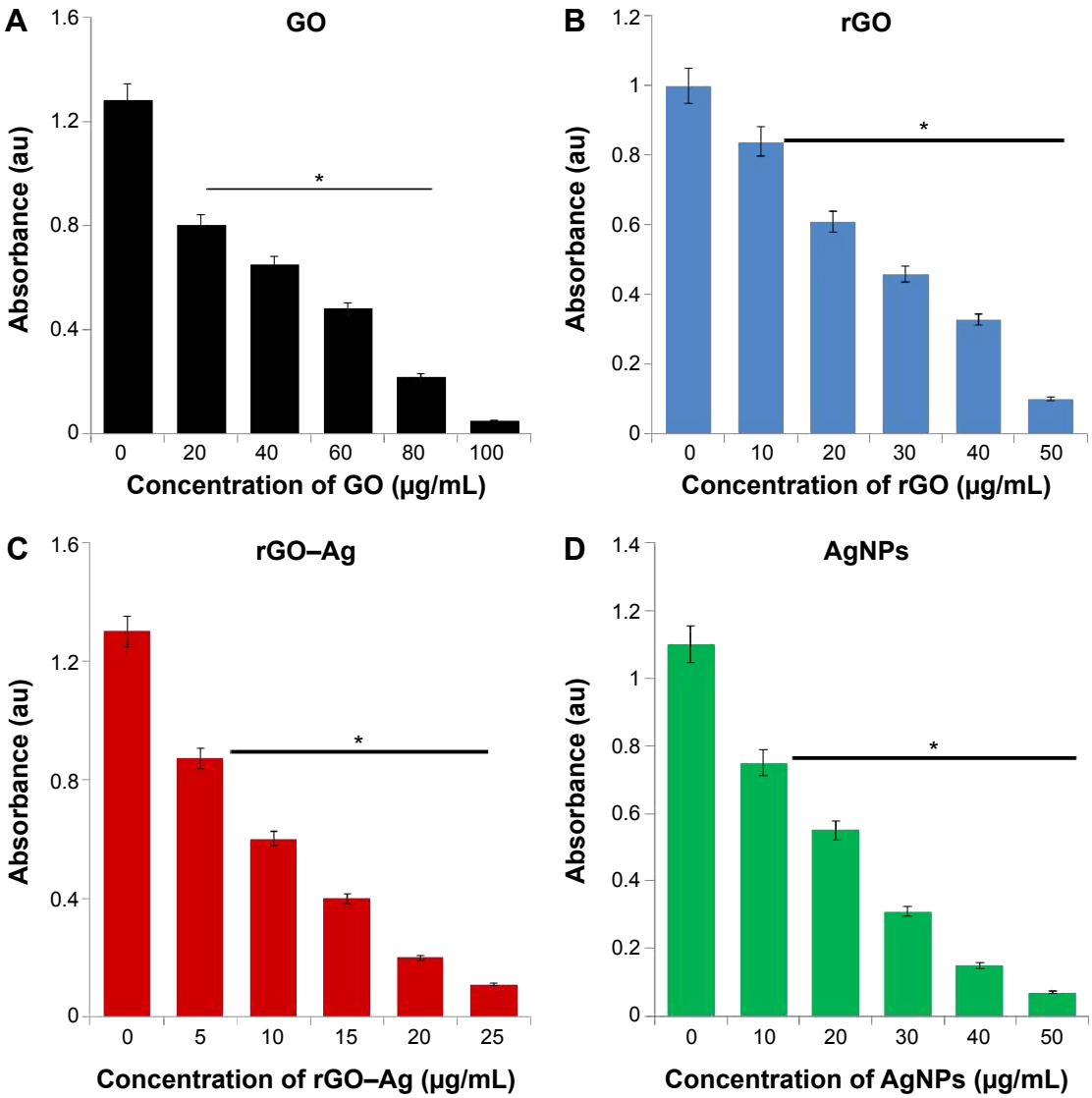

Figure 7 (**A**) Effects of graphene oxide (GO), (**B**) reduced graphene oxide (rGO), (**C**) rGO–Ag nanocomposite, and (**D**) Ag nanoparticles (AgNPs) on the viability of human ovarian cancer cells.

Notes: The viability of A2780 human ovarian cancer cells was determined after 24-hour exposure to different concentrations of GO, rGO, rGO–Ag nanocomposite, and AgNPs using the WST-8 assay. The results are expressed as the mean ± standard deviation of three independent experiments. A significant difference was observed above 50 μM. The viability of treated cells compared to the untreated cells by the Student's *t*-test (*$P<0.05$).

rGO, and AgNPs as controls. Figure 7 shows the results of the cell viability analysis. A dose-dependent inhibition of the cell viability is observed with GO in the range of 20–100 µg/mL with an IC_{50} of ~60 µg/mL (Figure 7A). Using rGO, a dose-dependent inhibition of the cell viability is observed in the range of 10–50 µg/mL with an IC_{50} of ~25 µg/mL (Figure 7B). With rGO–Ag, a dose-dependent inhibition of the cell viability is observed in the range of 5–25 µg/mL with an IC_{50} of ~12.5 µg/mL (Figure 7C). A dose-dependent inhibition of the cell viability is observed with AgNPs in the range of 10–50 µg/mL with an IC_{50} of ~20 µg/mL (Figure 7D). rGO–Ag is shown to have a more pronounced inhibitory effect on the cell viability than the other tested nanomaterials. Altogether, the results suggest that the rGO–Ag nanocomposite is a promising material for inhibiting the viability of ovarian cancer cells. Similarly, Hu et al[75] observed significant solubility and toxicity against HeLa cells using rGO–AgNP–folic acid. Earlier findings from other laboratories also support the reduced toxicity effect of GO observed in our results.[91,92] Akhavan et al[14] demonstrated effective photothermal therapy in cancer cells and observed that the activity of the transparent GO sheets was not as effective as the action of the rGO produced through the reduction by glucose in the presence of an Fe catalyst. In our previous studies, we also reported that GO is less toxic than rGO for several cancer and non-cancer cells.[16,44,67] Yu et al[45] reported the efficacy of a graphene/Ag nanocomposite in bacteria.[39] Recently, Fiorillo et al[15] using large GO flakes, observed a dose-dependent inhibition of tumor sphere formation; interestingly, neither small nor large GO flakes affected the viability of the bulk non-CSC population of the MCF7 cells indicating the selectivity of GO toward CSCs of ovarian, prostate, pancreatic, and lung cancers as well as glioblastoma. This is the first comprehensive study showing the efficacy of GO, rGO, rGO–Ag nanocomposite, and AgNPs. Based on the cell viability assay above, the results suggest that the obtained rGO–Ag nanocomposite has a stronger inhibitory effect than GO, rGO, and AgNPs.

Effect of rGO–Ag nanocomposite on cell morphology of ovarian cancer cells

Previous studies showed that the use of GO and rGO induce apoptosis in cancer and non-cancer cells. Therefore, we examined whether the addition of the rGO–Ag nanocomposite to A2780 cultures produced any pronounced effect on the cellular morphology. In addition, to support the results of the cell viability assay, we further evaluated the effect of GO, rGO, rGO–Ag nanocomposite, and AgNPs on the cell morphology of ovarian cancer cells. To this end, we selected the IC_{50} concentrations of GO, rGO, rGO–Ag nanocomposite, and AgNPs, and treated the cells for 24 hours. Figure 8 shows a photomicrograph composite of the A2780 cells incubated for 24 hours in the presence or absence (control) of the respective IC_{50} concentrations of GO, rGO, rGO–Ag nanocomposite,

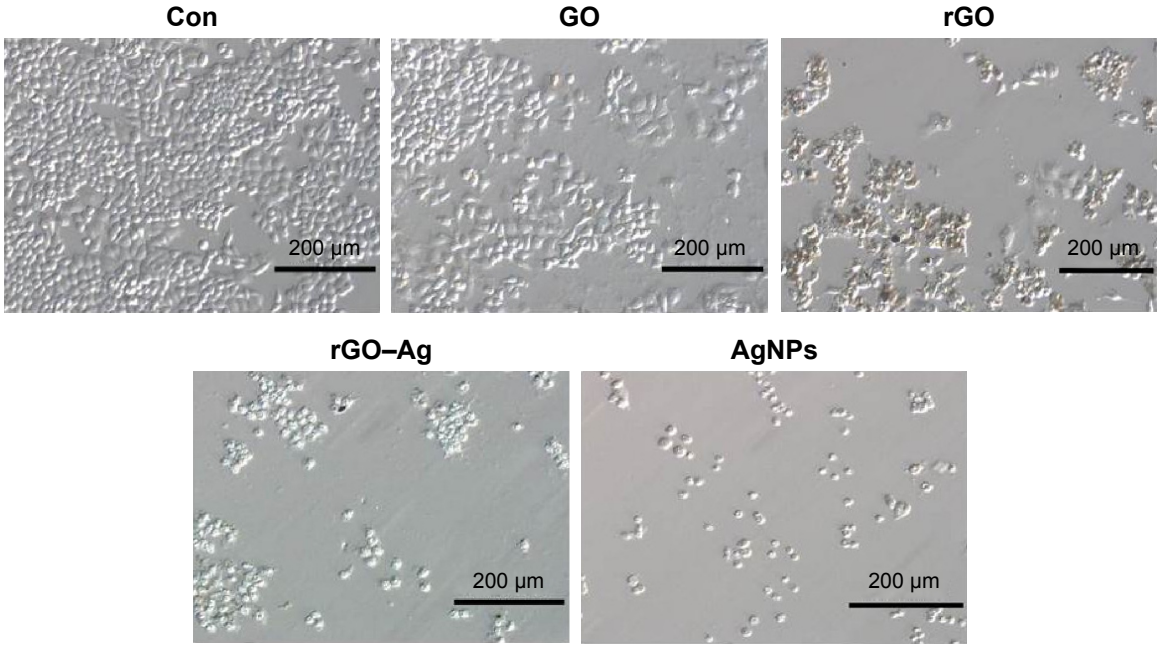

Figure 8 Morphology of human ovarian cancer cells treated with GO, rGO, rGO–Ag nanocomposite, and AgNPs.
Abbreviations: Con, control; GO, graphene oxide; rGO, reduced graphene oxide; AgNPs, silver nanoparticles.

and AgNPs. The control A2780 cells appear as small, round, dense clumps of cells with indistinct cell borders. A reduced number of cells and a significant effect on the cell morphology are observed in the A2780 cells treated with GO. The GO-treated cells look slightly different from those of the control group. A clear difference is observed between the rGO and rGO–Ag nanocomposite-treated cells and the control sample. The rGO and rGO–Ag nanocomposite-treated cells are denser and more oval, with shorter protrusions than those in the control cells. The AgNP-treated cells also show dramatic differences, but these are less evident than those observed on the rGO–Ag nanocomposite-treated cells. Similarly, Jaworski et al[93] reported the differential toxicity effect of GO and rGO in glioma cells. Interestingly, a severe effect on the morphology and number of the cells was observed in cells treated with rGO and rGO–Ag nanocomposite (Figure 8). With the exception of the control cells, all samples show a decrease in the number of cells after treatment with GO, rGO, rGO–Ag nanocomposite, and AgNPs. A more pronounced effect on cell growth is observed in the rGO–Ag nanocomposite-treated cells than on AgNP-, rGO-, and GO-treated cells. The order of degree of the cell growth inhibition is observed as rGO–Ag nanocomposite, AgNPs, rGO, and lastly GO.

Effect of rGO–Ag nanocomposite on membrane integrity

The measurement of the cell membrane integrity is widely used to assess the cytotoxicity of chemical agents used in cells.[94] Among several enzymatic assays, the measurement of the extracellular activity of LDH in the culture medium is routine for toxicity assays. In this experiment, we treated the cells with IC_{50} concentrations of GO, rGO, rGO–Ag nanocomposite, and AgNPs for 24 hours. The intracellular LDH molecules were released into the culture medium upon the damage of the cell membrane by the treatment with graphene nanomaterials.[16,44,93] The level of LDH in the culture media indicates the extent of damage caused by the agent. The results obtained from this experiment are consistent with those of the cell viability assays, indicating that the rGO–Ag nanocomposite causes a higher leakage of LDH than the other tested nanomaterials (Figure 9). Although all nanomaterials induce LDH leakage, the rGO–Ag nanocomposite has a remarkable response and a significant impact on the membrane integrity compared with the control sample. The cytotoxicity strongly depends on the type of graphene materials as well as on physical and chemical properties and the type and level of chemical functionalization.[10,14,16,24,44,95,96]

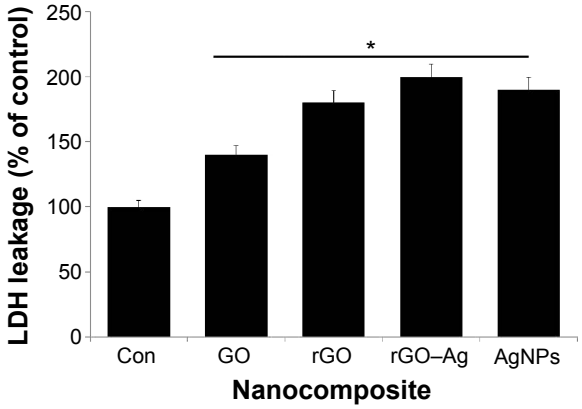

Figure 9 Effect of GO, rGO, rGO–Ag nanocomposite, and AgNPs on the leakage of LDH to culture supernatant of human ovarian cancer cells.
Notes: LDH activity is measured at 490 nm using the LDH cytotoxicity kit. The results are expressed as the mean ± standard deviation of three independent experiments. There was a significant difference in the LDH activity of rGO–Ag nanocomposite-treated cells compared to that of the untreated cells by the Student's *t*-test (*$P<0.05$).
Abbreviations: Con, control; GO, graphene oxide; rGO, reduced graphene oxide; AgNPs, silver nanoparticles; LDH, lactate dehydrogenase.

Impact of rGO–Ag nanocomposite on ROS generation

Several studies have reported the importance of ROS in cytotoxicity. Oxidative stress is one proposed toxicological mechanism of various nanomaterials, including graphene.[10,14,49] To investigate the effect of the rGO–Ag nanocomposite on ROS generation, the cells were treated with rGO–Ag nanocomposites and the other nanomaterials of GO, rGO, and AgNPs. The results clearly indicate that rGO–Ag profoundly affects ROS generation when compared to control. Although other nanomaterials also induce ROS generation, the effect of the rGO–Ag nanocomposite is considerably stronger (Figure 10). Our results are consistent with previous reports on various cancer cell lines with graphene and graphene-related materials. These results show the increased generation of ROS in rGO–Ag nanocomposite-treated cells, which may result from the high cellular uptake of the rGO nanocomposite.[97] Chang et al[48] reported that GO did not enter A549 cells and exerted no significant cytotoxic effects, but induced oxidative stress in cells at high concentrations. Lammel et al[98] demonstrated that GO was cytotoxic to HepG2 cells through the induction of plasma membrane damage and oxidative stress. Zhang et al[46] clearly demonstrated the role of ROS in the cytotoxicity of PC12 cells. Our previous studies also showed that GO and rGO induced significant oxidative stress in various cancer cells, including MCF-7 cells[17] and MDA-MB-231 human breast cancer cells.[16] Interestingly, this study shows that the toxicity of the rGO–Ag nanocomposite has a more dramatic effect on ROS generation than

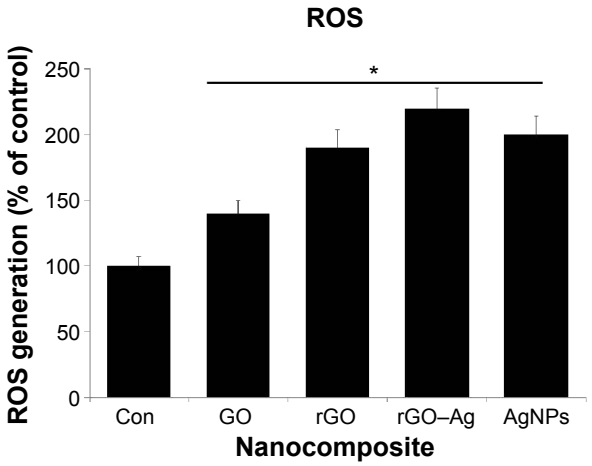

Figure 10 GO-, rGO-, rGO–Ag nanocomposite-, and AgNP-induced ROS generation in human ovarian cancer cells.
Notes: Relative fluorescence of 2′,7′-dichlorofluorescein was measured at the excitation wavelength of 485 nm and emission wavelength of 530 nm using a spectrofluorometer. The results are expressed as the mean ± standard deviation of three independent experiments. The treated groups showed statistically significant differences from the control group by the Student's *t*-test (*$P<0.05$).
Abbreviations: Con, control; GO, graphene oxide; rGO, reduced graphene oxide; AgNPs, silver nanoparticles; ROS, reactive oxygen species.

that of rGO, GO, or AgNPs. Thus, the mechanisms behind the cytotoxicity of the rGO–Ag nanocomposite may relate to oxidative stress.

Effect of rGO–Ag nanocomposite on the levels of MDA and GSH

Oxidative stress plays an important role in the cytotoxicity mechanism of nanomaterials. To support the oxidative responses of the rGO–Ag nanocomposite, we assayed the cellular levels using the two well-known biomarkers of pro-oxidant MDA and antioxidant GSH. The levels of MDA are shown in Figure 11A. In the cells treated with GO, rGO, rGO–Ag nanocomposite, and AgNPs, MDA increases from 0.5 nmol/mg protein to 1, 1.5, 2.5, and 2.0 nmol/mg protein, respectively, compared with that in control cells. These results suggest that the rGO–Ag nanocomposite significantly increases the intracellular production of MDA. Although all tested nanomaterials affected MDA production, the strongest effect is observed in rGO–Ag nanocomposite-treated cells.

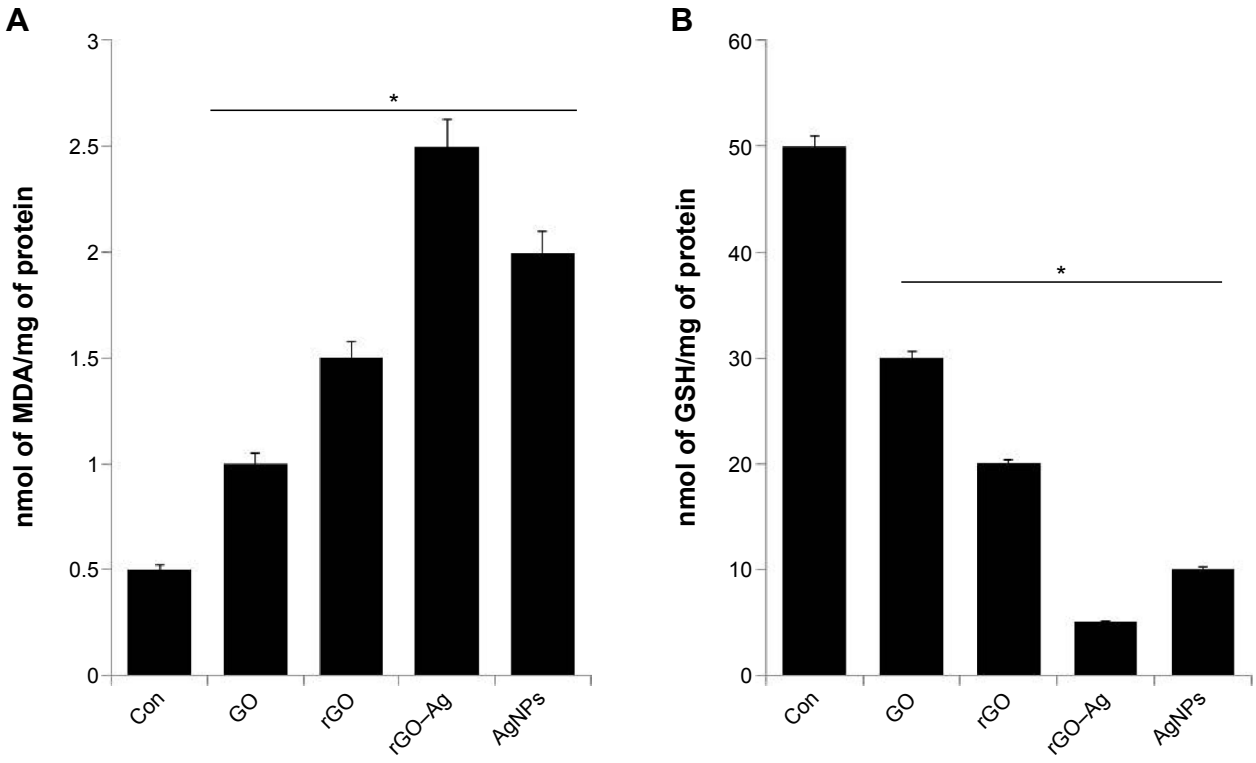

Figure 11 (**A**) Cellular MDA levels of A2780 cells exposure to GO, rGO, rGO–Ag nanocomposite, and AgNPs. (**B**) Cellular GSH levels of A2780 cells after exposure to GO, rGO, rGO–Ag nanocomposite, and AgNPs.
Notes: (**A**) A2780 cells were treated with the respective IC_{50} concentrations of GO, rGO, rGO–Ag nanocomposite, and AgNPs for 24 hours. After incubation, the cells were harvested and washed twice with an ice-cold PBS solution. The cells were collected and disrupted by ultrasonication for 5 minutes on ice. The concentration of MDA was measured on a microplate reader at a wavelength of 530 nm. (**B**) A2780 cells were treated with the respective IC_{50} concentrations of GO, rGO, rGO–Ag nanocomposite, and AgNPs for 24 hours. After incubation, the cells were harvested and washed twice with an ice-cold PBS solution. The cells were collected and disrupted by ultrasonication for 5 minutes on ice. The concentration of GSH was expressed as nmol per milligram of protein. The reaction was monitored at 405 nm in a microplate reader. *$P<0.05$.
Abbreviations: Con, control; IC, inhibitor concentration; MDA, malonaldehyde; GO, graphene oxide; rGO, reduced graphene oxide; AgNPs, silver nanoparticles; PBS, phosphate-buffered saline; GSH, glutathione.

In cells, an imbalance between pro-oxidant (MDA) and antioxidant (GSH) compounds may lead to oxidative stress.[68] Therefore, we examined the levels of GSH (Figure 11B). The GSH decreased from 50 to 30, 20, 5, and 10 in cells treated with GO, rGO, rGO–Ag nanocomposite, and AgNPs, respectively, when compared with the control cells. This suggests that the rGO–Ag nanocomposite reduces the intracellular GSH level more than the other tested nanomaterials do.

In this study, the oxidative stress was evaluated by the measurement of intracellular MDA and GSH levels. The levels of MDA indicated that the lipid peroxidation significantly increased when the cells were treated with the rGO–Ag nanocomposite. Interestingly, the amounts of intracellular MDA in cells treated with the rGO–Ag nanocomposite were twice that of the control cells whereas the intracellular GSH level of the cells treated with the rGO–Ag nanocomposite was four times lower than that of the control cells. This agrees with the suggestion from previous works that an imbalance between MDA and GSH compounds could lead to oxidative stress.[68] Recently, Dinh et al[99] reported that the antibacterial activity and mechanisms of Ag-decorated multi-walled CNTs induced toxicity in bacteria. They concluded that the significant antibacterial activity resulted from synergistic effects between AgNPs and multi-walled CNTs. Our data also suggest that the possible mechanism of the cell toxicity activity is related to the synergy between membrane stress and oxidative stress. Membrane stress is mediated by the direct physical contact of rGO and Ag with the cell membrane walls, while oxidative stress is caused by the induction of ROS mediated by the functionalized rGO and Ag materials.[99–101]

rGO–Ag nanocomposite-induced caspase-3 activity

ROS and caspases have been implicated as potential mediators of cell death.[102] Caspase-3, a cysteine protease, has been shown to be critical in Fas-mediated,[103] spontaneous,[104] and staurosporine-mediated[105] apoptosis. However, the mechanistic relationship remains unclear in the context of graphene and graphene-related material-induced toxicity. Therefore, we investigated the role of caspases in apoptosis induced by the ROS generated by rGO–Ag and other carbon nanomaterials. To determine the importance of caspase-3 activation in the apoptotic pathway of the cells, the cells were treated with respective IC_{50} concentrations of GO, rGO, rGO–Ag nanocomposite, and AgNPs. When the cells are treated for 24 hours, the activity of caspase-3 increases significantly compared to that of the control (Figure 12). However, as with the other biochemical assays, the rGO–Ag nanocomposite-treated culture shows a remarkably higher level of caspase-3 activity than cultures treated with other tested nanomaterials.

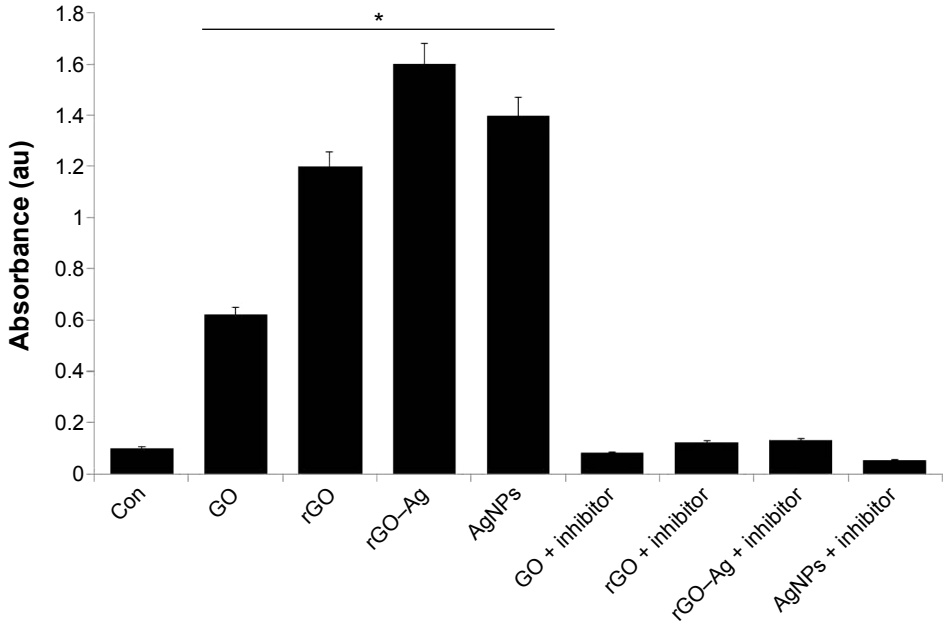

Figure 12 Effects of GO, rGO, rGO–Ag nanocomposite, and AgNPs on caspase-3 activity in human ovarian cancer cells.
Notes: Ovarian cancer cells were treated with GO, rGO, rGO–Ag nanocomposite, and AgNPs with or without the caspase-3 inhibitor Ac-DEVD-CHO for 24 hours. The concentration of p-nitroanilide released from the substrate was calculated from the absorbance at 405 nm. The results are expressed as the mean ± standard deviation of three separate experiments. The treated groups showed statistically significant differences from the control group by the Student's *t*-test (*$P<0.05$).
Abbreviations: Con, control; GO, graphene oxide; rGO, reduced graphene oxide; AgNPs, silver nanoparticles; Ac-DEVD-CHO, N-Ac-Asp-Glu-Val-Asp-CHO; Ac-DEVD-pNA, acetyl-Asp-Glu-Val-Asp p-nitroanilide.

Treatment with iron oxide NPs in MCF-7 cells revealed that the mode of cell death was apoptosis, mediated by the ROS-triggered mitochondrial pathway, as evidenced by the cleavage of the caspase-3 activity.[106] The activation signal of caspase-3 seemed to be through the induction of ROS; generally, toxic chemicals like iron oxide NPs,[107] cadmium, and mercury[108] induce ROS generation. Here, a similar phenomenon may occur for the caspase-3 activation by GO, rGO, rGO–Ag nanocomposite, and AgNPs. The activation of poly(ADP-ribose)polymerase cleavable protease, such as caspase 3-like protease, has been suggested to be promoted by ROS.[109] The results of this assay suggest that graphene materials cause the direct involvement of a caspase-family protease in ROS-induced apoptosis. In addition, we also show that the irreversible caspase-3 inhibitor prevents the caspase-3 activation.

rGO–Ag nanocomposite-induced apoptosis in ovarian cancer cells

The data from the previous experiments, such as the increased production of ROS and MDA and the reduced activity of the antioxidant enzymes and GSH, suggested that the rGO–Ag nanocomposite caused induced oxidative stress, which may result in cell damage and apoptosis via DNA damage. Therefore, this experiment was designed to address whether the rGO–Ag nanocomposite could induce DNA fragmentation by oxidative stress. The DNA fragmentation assay enables the assessment of cell death, which is a hallmark of apoptosis. To confirm the induction of apoptosis in A2780 cells, the cells were treated with GO, rGO, and rGO–Ag nanocomposite for 24 hours; the TUNEL analysis was performed on the treated cells. The results indicate that treatment with GO, rGO, and rGO–Ag nanocomposite causes the appearance of a significant number of TUNEL-positive A2780 cells, whereas no apoptotic cells are observed in the control (Figure 13A–C). Interestingly, the rGO–Ag nanocomposite-treated cells show an advanced degree of fragmentation when compared with the cells treated with other tested nanomaterials. This indicates that the cytotoxicity of the rGO–Ag nanocomposite is associated with the induction of apoptosis. Recently,

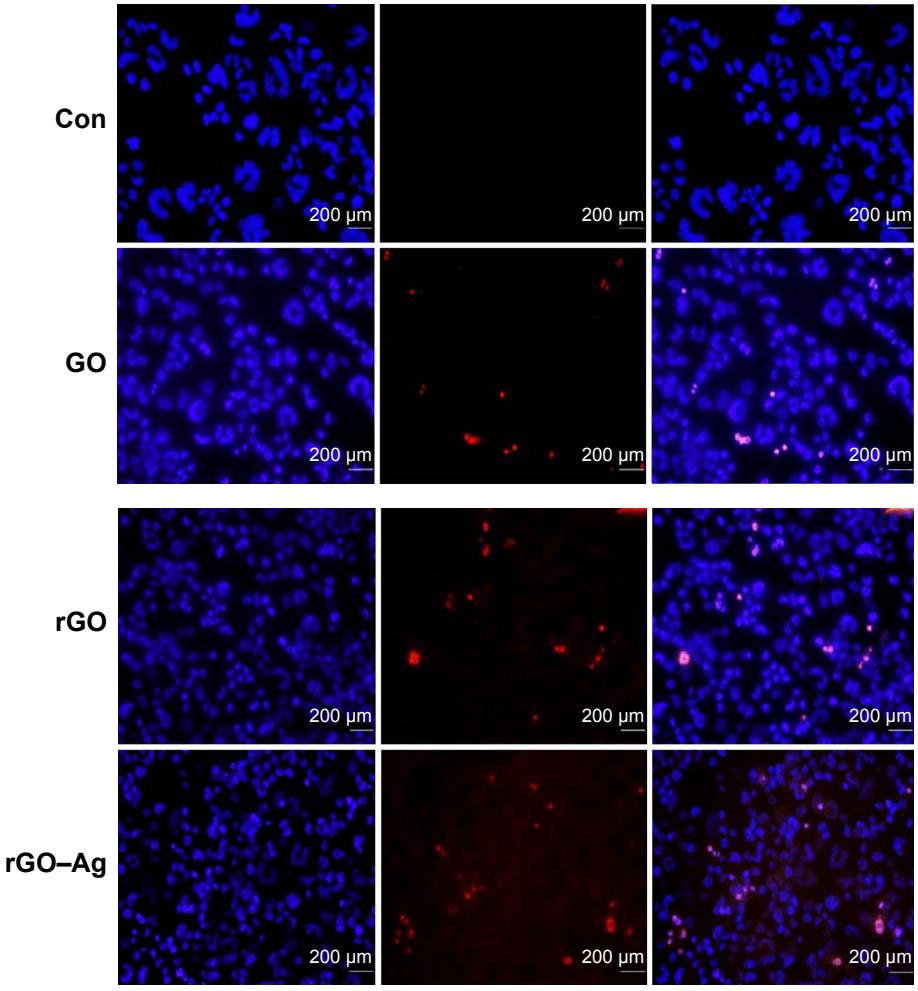

Figure 13 (*Continued*)

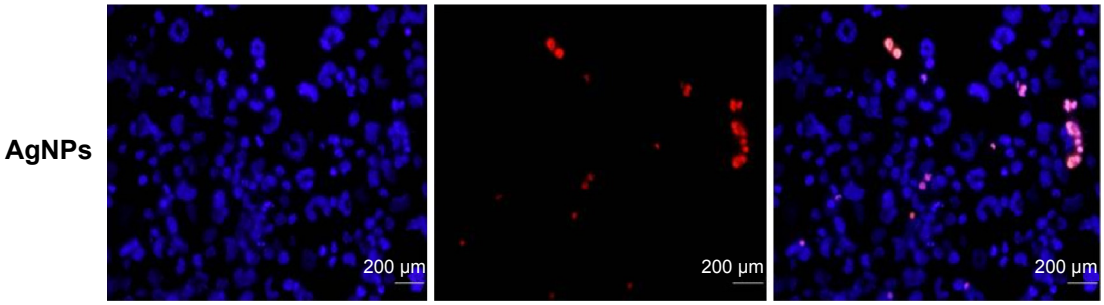

Figure 13 rGO–Ag nanocomposite-induced apoptosis in human ovarian cancer cells.
Notes: The cells were treated with respective IC_{50} concentrations of GO, rGO, rGO–Ag nanocomposite, and AgNPs for 24 hours. Apoptosis of human ovarian cancer cells after 24-hour treatment was assessed by the TUNEL assay; the nuclei were counterstained with DAPI. Representative images show apoptotic (fragmented) DNA (red staining) and the corresponding cell nuclei (blue staining).
Abbreviations: Con, control; GO, graphene oxide; rGO, reduced graphene oxide; AgNPs, silver nanoparticles.

Akhavan et al[14] observed that both DNA fragmentations and chromosomal aberrations in human mesenchymal stem cells treated with low concentration rGO–NPs were caused by penetration into the cells, which resulted in interactions between the penetrated nanosheets and the cell nuclei. Earlier studies suggested that carbon nanomaterials, including multi-walled CNTs and nanodiamonds, could induce the expression of chromosomal DNA-damage biomarkers, p53, MOGG-1, and Rad51, and DNA fragmentation in mouse embryonic stem cells and embryonic stem cells, respectively.[110,111] In our study, we observed similar DNA fragmentation in the cells treated with the rGO–Ag nanocomposite; the fragmentation is significantly higher than that in rGO-treated cells. Altogether, the data suggest that the rGO–Ag nanocomposite is a promising agent to inhibit the growth of cancer cells. The hypothetical mechanism is shown in Figure 14.

Conclusion

In this work, we demonstrated a simple, environmentally friendly, and dependable approach for the synthesis of rGO–Ag nanocomposites using the natural enzyme TAPE. The synthesized rGO–Ag nanocomposite was characterized by UV-Vis, FTIR, Raman spectroscopy, XRD, SEM, and TEM, which demonstrated that AgNPs with diameters of approximately 20 nm were deposited uniformly and compactly on rGO. Moreover, the rGO–Ag nanocomposite nanosheets showed excellent solubility and stability for more than 3 months. The rGO–Ag nanocomposite displayed significant cytotoxicity and showed highly effective apoptotic activity against ovarian cancer cells. The combined nanomaterials in our assays yielded a synergistic effect, which indicated that the combined process efficacy was higher than the sum of the individual efficacies of the individual nanomaterials. This novel formulation may aid the development of better

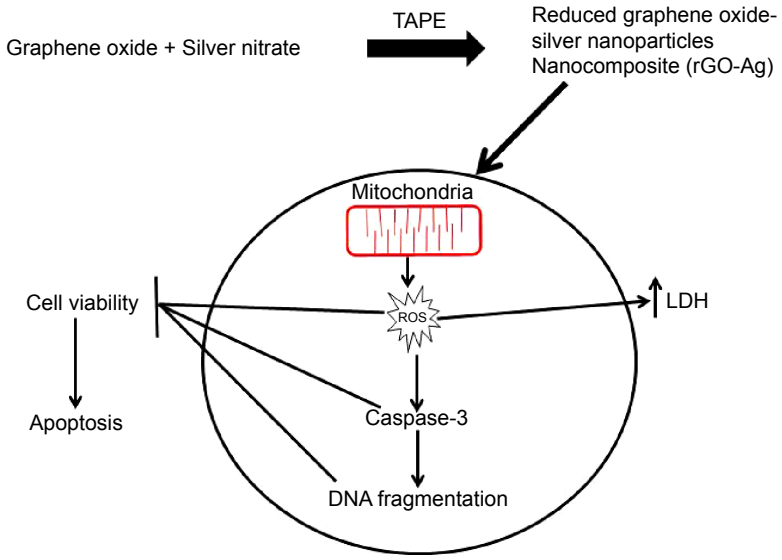

Figure 14 The hypothetical model for synthesis of rGO–Ag and its mechanisms in inducing cell death in human ovarian cancer cells.
Abbreviations: GO, graphene oxide; rGO, reduced graphene oxide; $AgNO_3$, silver nanoparticle; LDH, lactate dehydrogenase; TAPE, *Tilia amurensis* plant extracts; ROS, reactive oxygen species.

anticancer therapeutics and could provide new treatments for the cancer and CSC-targeted cancer therapies.

Acknowledgments

This work was supported by the KU-Research Professor Program of Konkuk University. Dr Sangiliyandi Gurunathan was supported by a Konkuk University KU-full-time Professorship. This work was also supported by the Woo Jang-Choon project (PJ007849) and Biogreen 21 (PJ011328) from the Rural Development Administration (RDA), Republic of Korea.

Disclosure

The authors report no conflicts of interest in this work.

References

1. Geim AK, Novoselov KS. The rise of graphene. *Nat Mater*. 2007;6(3):183–191.
2. Lee CH, Hsue YC, Chen RB, Li TS, Lin MF. Electronic structures of finite double-walled carbon nanotubes in a magnetic field. *J Phys Condens Matter*. 2008;20(7):075213.
3. Novoselov KS, Geim AK, Morozov SV, et al. Electric field effect in atomically thin carbon films. *Science*. 2004;306(5696):666–669.
4. Stoller MD, Park SJ, Zhu YW, An JH, Ruoff RS. Graphene-based ultracapacitors. *Nano Lett*. 2008;8(10):3498–3502.
5. Li D, Muller MB, Gilje S, Kaner RB, Wallace GG. Processable aqueous dispersions of graphene nanosheets. *Nature Nanotechnol*. 2008;3(2):101–105.
6. Khan JM, Kurchania R, Sethi VK. Synthesis and characterization of two dimensional graphene lamellae based PAn nanocomposites. *Thin Solid Films*. 2010;519(3):1059–1065.
7. He YM, Chen WJ, Gao CT, Zhou JY, Li XD, Xie EQ. An overview of carbon materials for flexible electrochemical capacitors. *Nanoscale*. 2013;5(19):8799–8820.
8. Hui KS, Hui KN, Dinh DA, et al. Green synthesis of dimension-controlled silver nanoparticle-graphene oxide with in situ ultrasonication. *Acta Mater*. 2014;64:326–332.
9. Akhavan O, Ghaderi E. Toxicity of graphene and graphene oxide nanowalls against bacteria. *ACS Nano*. 2010;4(10):5731–5736.
10. Gurunathan S, Han JW, Dayem AA, Eppakayala V, Kim JH. Oxidative stress-mediated antibacterial activity of graphene oxide and reduced graphene oxide in Pseudomonas aeruginosa. *Int J Nanomed*. 2012;7:5901–5914.
11. Hu WB, Peng C, Luo WJ, et al. Graphene-based antibacterial paper. *ACS Nano*. 2010;4(7):4317–4323.
12. Lu CH, Yang HH, Zhu CL, Chen X, Chen GN. A graphene platform for sensing biomolecules. *Angew Chem Int Edit*. 2009;48(26):4785–4787.
13. Sun XM, Liu Z, Welsher K, et al. Nano-graphene oxide for cellular imaging and drug delivery. *Nano Res*. 2008;1(3):203–212.
14. Akhavan O, Ghaderi E, Aghayee S, Fereydooni Y, Talebi A. The use of a glucose-reduced graphene oxide suspension for photothermal cancer therapy. *J Mater Chem*. 2012;22(27):13773–13781.
15. Fiorillo M, Verre AF, Iliut M, et al. Graphene oxide selectively targets cancer stem cells, across multiple tumor types: implications for non-toxic cancer treatment, via "differentiation-based nano-therapy". *Oncotarget*. 2015;6(6):3553–3562.
16. Gurunathan S, Han J, Park JH, Kim JH. An in vitro evaluation of graphene oxide reduced by Ganoderma spp. in human breast cancer cells (MDA-MB-231). *Int J Nanomed*. 2014;9:1783–1797.
17. Gurunathan S, Han JW, Eppakayala V, Kim JH. Green synthesis of graphene and its cytotoxic effects in human breast cancer cells. *Int J Nanomed*. 2013;8:1015–1027.
18. Zhou L, Wang W, Tang J, Zhou JH, Jiang HJ, Shen J. Graphene oxide noncovalent photosensitizer and Its anticancer activity In vitro. *Chem-Eur J*. 2011;17(43):12084–12091.
19. Hu Z, Huang YD, Sun SF, et al. Visible light driven photodynamic anticancer activity of graphene oxide/TiO2 hybrid. *Carbon*. 2012;50(3):994–1004.
20. Wang C, Wu CY, Zhou XJ, et al. Enhancing cell nucleus accumulation and DNA cleavage activity of anti-cancer drug via graphene quantum dots. *Sci Rep-Uk*. 2013;3:2852.
21. Cheng RM, Zou RT, Ou SJ, et al. Graphene oxide complex as a pH-sensitive antitumor drug. *Polym Chem*. 2015;6(13):2401–2406.
22. Liu GD, Shen H, Mao JN, et al. Transferrin modified graphene oxide for glioma-targeted drug delivery: in vitro and in vivo evaluations. *ACS Appl Mater Interfaces*. 2013;5(15):6909–6914.
23. Yun SW, Cha JR, Gong MS. Easy preparation of nanosilver-decorated graphene using silver carbamate by microwave irradiation and their properties. *B Korean Chem Soc*. 2014;35(8):2251–2256.
24. Gurunathan S, Han JW, Kim ES, Park JH, Kim JH. Reduction of graphene oxide by resveratrol: a novel and simple biological method for the synthesis of an effective anticancer nanotherapeutic molecule. *Int J Nanomed*. 2015;10:2951–2969.
25. Khanra P, Kuila T, Kim NH, Bae SH, Yu DS, Lee JH. Simultaneous bio-functionalization and reduction of graphene oxide by baker's yeast. *Chem Eng J*. 2012;183:526–533.
26. Kim YK, Kim MH, Min DH. Biocompatible reduced graphene oxide prepared by using dextran as a multifunctional reducing agent. *Chem Commun*. 2011;47(11):3195–3197.
27. Stankovich S, Piner RD, Chen XQ, Wu NQ, Nguyen ST, Ruoff RS. Stable aqueous dispersions of graphitic nanoplatelets via the reduction of exfoliated graphite oxide in the presence of poly(sodium 4-styrenesulfonate). *J Mater Chem*. 2006;16(2):155–158.
28. Gurunathan S, Han JW, Eppakayala V, Dayem AA, Kwon DN, Kim JH. Biocompatibility effects of biologically synthesized graphene in primary mouse embryonic fibroblast cells. *Nanoscale Res Lett*. 2013;8(1):393.
29. Fernandez-Merino MJ, Guardia L, Paredes JI, et al. Vitamin C is an ideal substitute for hydrazine in the reduction of graphene oxide suspensions. *J Phys Chem C*. 2010;114(14):6426–6432.
30. Gao J, Liu F, Liu YL, Ma N, Wang ZQ, Zhang X. Environment-friendly method to produce graphene that employs vitamin C and amino acid. *Chem Mater*. 2010;22(7):2213–2218.
31. Esfandiar A, Akhavan O, Irajizad A. Melatonin as a powerful bio-antioxidant for reduction of graphene oxide. *J Mater Chem*. 2011;21(29):10907–10914.
32. Gurunathan S, Han J, Kim JH. Humanin: A novel functional molecule for the green synthesis of graphene. *Colloids Surf B Biointerfaces*. 2013;111:376–383.
33. Akhavan O, Ghaderi E. Escherichia coli bacteria reduce graphene oxide to bactericidal graphene in a self-limiting manner. *Carbon*. 2012;50(5):1853–1860.
34. Gurunathan S, Han JW, Eppakayala V, Kim JH. Microbial reduction of graphene oxide by escherichia coli: a green chemistry approach. *Colloids Surf B Biointerfaces*. 2013;102:772–777.
35. Salas EC, Sun ZZ, Luttge A, Tour JM. Reduction of graphene oxide via bacterial respiration. *ACS Nano*. 2010;4(8):4852–4856.
36. Stensberg MC, Wei Q, McLamore ES, Porterfield DM, Wei A, Sepulveda MS. Toxicological studies on silver nanoparticles: challenges and opportunities in assessment, monitoring and imaging. *Nanomedicine (Lond)*. 2011;6(5):879–898.
37. Baik JM, Lee SJ, Moskovits M. Polarized surface-enhanced raman spectroscopy from molecules adsorbed in nano-gaps produced by electromigration in silver nanowires. *Nano Lett*. 2009;9(2):672–676.
38. Christopher P, Linic S. Engineering selectivity in heterogeneous catalysis: Ag nanowires as selective ethylene epoxidation catalysts. *J Am Chem Soc*. 2008;130(34):11264–11265.
39. Yang EH. Engineered low-dimensional nanomaterials for sensors, actuators, and electronics. *J Micro-Nanolith Mem*. 2010;9(4):041103.

40. Lee KS, El-Sayed MA. Gold and silver nanoparticles in sensing and imaging: sensitivity of plasmon response to size, shape, and metal composition. *J Phys Chem B*. 2006;110(39):19220–19225.
41. Sriram MI, Kanth SB, Kalishwaralal K, Gurunathan S. Antitumor activity of silver nanoparticles in dalton's iymphoma ascites tumor model. *Int J Nanomedicine*. 2010;5:753–762.
42. AshaRani PV, Low Kah Mun G, Hande MP, Valiyaveettil S. Cytotoxicity and genotoxicity of silver nanoparticles in human cells. *ACS Nano*. 2009;3(2):279–290.
43. Kalishwaralal K, BarathManiKanth S, Pandian SRK, Deepak V, Gurunathan S. Silver nano – a trove for retinal therapies. *J Control Release*. 2010;145(2):76–90.
44. Gurunathan S, Han JW, Eppakayala V, Jeyaraj M, Kim JH. Cytotoxicity of biologically synthesized silver nanoparticles in MDA-MB-231 human breast cancer cells. *Biomed Res Int*. 2013;2013:535796.
45. Yu L, Zhang YT, Zhang B, Liu JD. Enhanced antibacterial activity of silver nanoparticles/halloysite nanotubes/graphene nanocomposites with sandwich-like structure. *Sci Rep*. 2014;4:45–51.
46. Zhang YB, Ali SF, Dervishi E, et al. Cytotoxicity effects of graphene and single-wall carbon nanotubes in neural phaeochromocytoma-derived PC12 cells. *ACS Nano*. 2010;4(6):3181–3186.
47. Wang K, Ruan J, Song H, et al. Biocompatibility of graphene oxide. *Nanoscale Res Lett*. 2011;6(1):8.
48. Chang YL, Yang ST, Liu JH, et al. In vitro toxicity evaluation of graphene oxide on A549 cells. *Toxicol Lett*. 2011;200(3):201–210.
49. Liu L, Liu J, Wang Y, Yan X, Sun DD. Facile synthesis of monodispersed silver nanoparticles on graphene oxide sheets with enhanced antibacterial activity. *New J Chem*. 2011;35(7):1418–1423.
50. You JM, Kim D, Jeon S. Electrocatalytic Reduction of H2O2 on Thiolate graphene oxide covalently to bonded palladium nanoparticles. *J Nanosci Nanotechnol*. 2012;12(5):3943–3949.
51. Zhu YG, Cao GS, Sun CY, et al. Design and synthesis of NiO nanoflakes/graphene nanocomposite as high performance electrodes of pseudocapacitor. *RSC Adv*. 2013;3(42):19409–19415.
52. Chook SW, Chia CH, Zakaria S, et al. Antibacterial performance of Ag nanoparticles and AgGO nanocomposites prepared via rapid microwave-assisted synthesis method. *Nanoscale Res Lett*. 2012; 7(1):541.
53. Shao YL, Wang HZ, Zhang QH, Li YG. High-performance flexible asymmetric supercapacitors based on 3D porous graphene/MnO2 nanorod and graphene/Ag hybrid thin-film electrodes. *J Mater Chem C*. 2013;1(6):1245–1251.
54. Pasricha R, Gupta S, Srivastava AK. A facile and novel synthesis of Ag-graphene-based nanocomposites. *Small*. 2009;5(20):2253–2259.
55. Zhang Z, Xu FG, Yang WS, et al. A facile one-pot method to high-quality Ag-graphene composite nanosheets for efficient surface-enhanced Raman scattering. *Chem Commun*. 2011;47(22):6440–6442.
56. Lightcap IV, Kosel TH, Kamat PV. Anchoring semiconductor and metal nanoparticles on a two-dimensional catalyst mat. storing and shuttling electrons with reduced graphene oxide. *Nano Lett*. 2010;10(2): 577–583.
57. Liu S, Tian JQ, Wang L, Li HL, Zhang YW, Sun XP. Stable aqueous dispersion of graphene nanosheets: noncovalent functionalization by a polymeric reducing agent and their subsequent decoration with Ag nanoparticles for enzymeless hydrogen peroxide detection. *Macromolecules*. 2010;43(23):10078–10083.
58. Shen JF, Shi M, Yan B, Ma HW, Li N, Ye MX. One-pot hydrothermal synthesis of Ag-reduced graphene oxide composite with ionic liquid. *J Mater Chem*. 2011;21(21):7795–7801.
59. Dinh DA, Hui KS, Hui KN, et al. Green synthesis of high conductivity silver nanoparticle-reduced graphene oxide composite films. *Appl Surf Sci*. 2014;298:62–67.
60. Baba T, Convery PA, Matsumura N, et al. Epigenetic regulation of CD133 and tumorigenicity of CD133+ ovarian cancer cells. *Oncogene*. 2009;28(2):209–218.
61. Burgos-Ojeda D, Rueda BR, Buckanovich RJ. Ovarian cancer stem cell markers: Prognostic and therapeutic implications. *Cancer Lett*. 2012; 322(1):1–7.
62. Pasukoniene V, Mlynska A, Steponkiene S, et al. Accumulation and biological effects of cobalt ferrite nanoparticles in human pancreatic and ovarian cancer cells. *Medicina-Lithuania*. 2014;50(4): 237–244.
63. Deepak V, Umamaheshwaran PS, Guhan K, et al. Synthesis of gold and silver nanoparticles using purified URAK. *Colloids Surf B Biointerfaces*. 2011;86(2):353–358.
64. Gurunathan S, Kalishwaralal K, Vaidyanathan R, et al. Biosynthesis, purification and characterization of silver nanoparticles using escherichia coli. *Colloids Surf B Biointerfaces*. 2009;74(1):328–335.
65. Gurunathan S, Han JW, Kim E, Kwon DN, Park JK, Kim JH. Enhanced green fluorescent protein-mediated synthesis of biocompatible graphene. *J Nanobiotechnology*. 2014;12:41.
66. Hummers WS, Offeman RE. Preparation of graphitic oxide. *J Am Chem Soc*. 1958;80:1339.
67. Gurunathan S, Han JW, Eppakayala V, Kim JH. Biocompatibility of microbially reduced graphene oxide in primary mouse embryonic fibroblast cells. *Colloids Surf B Biointerfaces*. 2013;105:58–66.
68. Wang FG, Liu SR, Shen YQ, et al. Protective effects of N-acetylcysteine on cisplatin-induced oxidative stress and DNA damage in HepG2 cells. *Exp Ther Med*. 2014;8(6):1939–1945.
69. de Faria AF, Martinez DS, Meira SM, et al. Anti-adhesion and antibacterial activity of silver nanoparticles supported on graphene oxide sheets. *Colloids Surf B Biointerfaces*. 2014;113:115–124.
70. Li J, Liu CY. Ag/Graphene heterostructures: synthesis, characterization and optical properties. *Eur J Inorg Chem*. 2010;8:1244–1248.
71. Yuan XJ, Chai YQ, Yuan R, Zhao Q, Yang CL. Functionalized graphene oxide-based carbon paste electrode for potentiometric detection of copper ion(II). *Anal Methods*. 2012;4(10):3332–3337.
72. Xu C, Wang X. Fabrication of flexible metal-nanoparticte film using graphene oxide sheets as substrates. *Small*. 2009;5;19:2212–2217.
73. Shen JF, Shi M, Li N, et al. Facile synthesis and application of Ag-chemically converted graphene nanocomposite. *Nano Res*. 2010;3(5): 339–349.
74. Al-Marri AH, Khan M, Khan M, et al. Pulicaria glutinosa extract: a toolbox to synthesize highly reduced graphene oxide-silver nanocomposites. *Int J Mol Sci*. 2015;16(1):1131–1142.
75. Hu CF, Liu YL, Qin JL, et al. Fabrication of reduced graphene oxide and sliver nanoparticle hybrids for raman detection of absorbed folic acid: a potential cancer diagnostic probe. *ACS Appl Mater Interfaces*. 2013;5(11):4760–4768.
76. Zhou Z, He DL, Guo YN, et al. Fabrication of polyaniline-silver nanocomposites by chronopotentiometry in different ionic liquid microemulsion systems. *Thin Solid Films*. 2009;517(24):6767–6771.
77. Marcano DC, Kosynkin DV, Berlin JM, et al. Improved synthesis of graphene oxide. *ACS Nano*. 2010;4(8):4806–4814.
78. Zuo PP, Feng HF, Xu ZZ, et al. Fabrication of biocompatible and mechanically reinforced graphene oxide-chitosan nanocomposite films. *Chem Cent J*. 2013;7:39.
79. Zhu YW, Murali S, Cai WW, et al. Graphene and graphene oxide: synthesis, properties, and applications. *Adv Mater*. 2010;22(35): 3906–3924.
80. Nethravathi C, Rajamathi M. Chemically modified graphene sheets produced by the solvothermal reduction of colloidal dispersions of graphite oxide. *Carbon*. 2008;46(14):1994–1998.
81. Yuan WH, Gu YJ, Li L. Green synthesis of graphene/Ag nanocomposites. *Appl Surf Sci*. 2012;261:753–758.
82. Jeong BW, Ihm J, Lee GD. Stability of dislocation defect with two pentagon-heptagon pairs in graphene. *Phys Rev B*. 2008;78(16):165403.
83. Lian CX, Tahy K, Fang T, Li GW, Xing HG, Jena D. Quantum transport in graphene nanoribbons patterned by metal masks. *Appl Phys Lett*. 2010;96(10):103–109.
84. Yun H, Kim JD, Choi HC, Lee CW. Antibacterial activity of CNT-Ag and GO-Ag nanocomposites against gram-negative and gram-positive bacteria. *B Korean Chem Soc*. 2013;34(11):3261–3264.
85. Faria AF, Martinez DST, Moraes ACM, et al. Unveiling the role of oxidation debris on the surface chemistry of graphene through the anchoring of Ag nanoparticles. *Chem Mater*. 2012;24(21):4080–4087.

86. Ferrari AC, Meyer JC, Scardaci V, et al. Raman spectrum of graphene and graphene layers. *Phys Rev Lett*. 2006;97(18):187401.
87. Niyogi S, Bekyarova E, Itkis ME, et al. Spectroscopy of Covalently Functionalized Graphene. *Nano Lett*. 2010;10(10):4061–4066.
88. Akhavan O, Ghaderi E. Photocatalytic reduction of graphene oxide nanosheets on TiO2 thin film for photoinactivation of bacteria in solar light irradiation. *J Phys Chem C*. 2009;113(47):20214–20220.
89. Stankovich S, Dikin DA, Piner RD, et al. Synthesis of graphene-based nanosheets via chemical reduction of exfoliated graphite oxide. *Carbon*. 2007;45(7):1558–1565.
90. Wang P, Liu ZG, Chen X, Meng FL, Liu JH, Huang XJ. UV irradiation synthesis of an Au-graphene nanocomposite with enhanced electrochemical sensing properties. *J Mater Chem A*. 2013;1(32):9189–9195.
91. Liao KH, Lin YS, Macosko CW, Haynes CL. Cytotoxicity of graphene oxide and graphene in human erythrocytes and skin fibroblasts. *ACS Appl Mater Interfaces*. 2011;3(7):2607–2615.
92. Ruiz ON, Fernando KAS, Wang BJ, et al. Graphene oxide: a nonspecific enhancer of cellular growth. *ACS Nano*. 2011;5(10):8100–8107.
93. Jaworski S, Sawosz E, Grodzik M, et al. In vitro evaluation of the effects of graphene platelets on glioblastoma multiforme cells. *Int J Nanomed*. 2013;8:413–420.
94. Cho MH, Niles A, Huang RL, et al. A bioluminescent cytotoxicity assay for assessment of membrane integrity using a proteolytic biomarker. *Toxicol In Vitro*. 2008;22(4):1099–1106.
95. Sasidharan A, Panchakarla LS, Chandran P, et al. Differential nano-bio interactions and toxicity effects of pristine versus functionalized graphene. *Nanoscale*. 2011;3(6):2461–2464.
96. Yue H, Wei W, Yue ZG, et al. The role of the lateral dimension of graphene oxide in the regulation of cellular responses. *Biomaterials*. 2012;33(16):4013–4021.
97. Chowdhury SM, Lalwani G, Zhang KV, Yang JY, Neville K, Sitharaman B. Cell specific cytotoxicity and uptake of graphene nanoribbons. *Biomaterials*. 2013;34(1):283–293.
98. Lammel T, Boisseaux P, Fernandez-Cruz ML, Navas JM. Internalization and cytotoxicity of graphene oxide and carboxyl graphene nanoplatelets in the human hepatocellular carcinoma cell line Hep G2. *Particle Fibre Toxicol*. 2013;10:27.
99. Dinh NX, Quy NV, Huy TQ, Le AT. Decoration of silver nanoparticles on multiwalled carbon nanotubes: antibacterial mechanism and ultrastructural analysis. *J Nanomater*. 2015;2015:814379.
100. Shvedova AA, Pietroiusti A, Fadeel B, Kagan VE. Mechanisms of carbon nanotube-induced toxicity: focus on oxidative stress. *Toxicol Appl Pharm*. 2012;261(2):121–133.
101. Vecitis CD, Zodrow KR, Kang S, Elimelech M. Electronic-structure-dependent bacterial cytotoxicity of single-walled carbon nanotubes. *ACS Nano*. 2010;4(9):5471–5479.
102. Higuchi M, Honda T, Proske RJ, Yeh ETH. Regulation of reactive oxygen species-induced apoptosis and necrosis by caspase 3-like proteases. *Oncogene*. 1998;17(21):2753–2760.
103. Schlegel J, Peters I, Orrenius S, et al. CPP32/apopain is a key interleukin 1 beta converting enzyme-like protease involved in fas-mediated apoptosis. *J Biol Chem*. 1996;271(4):1841–1844.
104. Nicholson DW, Ali A, Thornberry NA, et al. Identification and inhibition of the ICE/CED-3 protease necessary for mammalian apoptosis. *Nature*. 1995;376(6535):37–43.
105. Jacobsen MD, Weil M, Raff MC. Role of Ced-3/ICE-family proteases in staurosporine-induced programmed cell death. *J Cell Biol*. 1996;133(5):1041–1051.
106. Alarifi S, Ali D, Alkahtani S, Alhader MS. Iron oxide nanoparticles induce oxidative stress, DNA damage, and caspase activation in the human breast cancer cell line. *Biol Trace Elem Res*. 2014;159(1–3):416–424.
107. Alarifi S, Ali D, Alakhtani S, Al Suhaibani ES, Al-Qahtani AA. Reactive oxygen species-mediated DNA damage and apoptosis in human skin epidermal cells after exposure to nickel nanoparticles. *Biol Trace Elem Res*. 2014;157(1):84–93.
108. Park EJ, Park K. Induction of reactive oxygen species and apoptosis in BEAS-2B cells by mercuric chloride. *Toxicol In Vitro*. 2007;21(5):789–794.
109. McGowan AJ, Ruiz-Ruiz MC, Gorman AM, Lopez-Rivas A, Cotter TG. Reactive oxygen intermediate(s) (ROI): common mediator(s) of poly(ADP-ribose)polymerase (PARP) cleavage and apoptosis. *FEBS Lett*. 1996;392(3):299–303.
110. Xing Y, Xiong W, Zhu L, Osawa E, Hussin S, Dai L. DNA damage in embryonic stem cells caused by nanodiamonds. *ACS Nano*. 2011;5(3):2376–2384.
111. Zhu L, Chang DW, Dai L, Hong Y. DNA damage induced by multiwalled carbon nanotubes in mouse embryonic stem cells. *Nano Lett*. 2007;7(12):3592–3597.